MULTIMODE FABRY-PEROT LASER DIODES: MODELING AND SIMULATION OF MODE PARTITIONING NOISE IN FIBRE-OPTIC COMMUNICATION LINKS

MULTIMODE FABRY-PEROT LASER DIODES: MODELING AND SIMULATION OF MODE PARTITIONING NOISE IN FIBRE-OPTIC COMMUNICATION LINKS

BY

MENGYU RAN, B.Sc.

A THESIS

SUBMITTED TO THE DEPARTMENT OF ELECTRICAL & COMPUTER ENGINEERING

AND THE SCHOOL OF GRADUATE STUDIES

OF MCMASTER UNIVERSITY

IN PARTIAL FULFILMENT OF THE REQUIREMENTS

FOR THE DEGREE OF

MASTER OF APPLIED SCIENCE

© Copyright by Mengyu Ran, September 2008

All Rights Reserved

Master of Applied Science (2008) McMaster University

(Electrical & Computer Engineering) Hamilton, Ontario, Canada

TITLE: MULTIMODE FABRY-PEROT LASER DIODES: MODELING AND SIMULATION OF MODE PARTITIONING NOISE IN FIBRE-OPTIC COMMUNICATION LINKS

AUTHOR: Mengyu Ran

B.Sc., (Electrical Engineering)

University of Saskatchewan, SK, Canada

SUPERVISOR: Dr. Weiping Huang

NUMBER OF PAGES: x, 54

This dissertation is dedicated to my family for all the wonderful things they do for me and supporting me all the way.

Abstract

The FP multimode semiconductor laser has lightened up a new field of optical communication technology in the past two decades. Numerical modeling of its physical behaviours and transient response has been discussed previously in literature, mostly by constructing the multimode rate equations. Rate equations are very helpful in studying and predicting the average photon and carrier transient response and relaxation oscillation. However, their deficiency in statistical photon fluctuation limits the function of describing stochastic power shifted from main mode to other side modes. Therefore, a noise driven model with conjunction of optical fibre and photodiode is built to form an optical communication system in the simulation scope.

The multimode nature of FP lasers causes several problems such as mode partitioning noise (MPN), intersymbol interference (ISI), and frequency chirping, among which mode partitioning noise is the most serious of the concern in this discussion. The stereotype analytical measurement of MPN power penalty is based on several assumptions on the received waveform shape and power distribution spectrum, which limits its fields of application and accuracy. This work develops a numerical solution to power penalty due to MPN, and it can be employed to any multimode laser diode models regardless of the received signal shape and power distribution

spectrum.

In conclusion, the MPN power penalty is a significant profile of evaluating system perform in fibre-optic communication links. It highly depends on shape of power distribution spectrum, number of modes, length of fibre, and pattern of signal waveform.

Acknowledgements

My heartfelt gratitude to Weiping Huang for persevering with me as my supervisor throughout the past two years with his vital encouragement and support.

The members of my dissertation committee, Weiping Huang, Xun Li, Shiva Kumar, have generously given their time and expertise to better my work. I thank them for their assistance and understanding.

I am grateful to my family who have been unconditionally supportive throughout the time. Without them this work would of never happened.

My thanks must go also to my friends and colleagues Lin Han, Jianwei Mu and Yanping Xi, who shared their professional opinions and experiences with me.

I must acknowledge as well all Electrical and Computer Engineering faculty members and staff, especially Cheryl Gies for her patient assistance and advice.

Contents

List of Figures

Chapter 1

Introduction

Laser diodes are widely used in modern telecommunications and fiber-optic communication systems. The laser diode, which plays a significant role as the transmitter, requires precisely defined wavelength, spectral width, and static and dynamic properties. Because of the high operation stability and narrow spectral width, the nearly single mode lasers such as distributed feedback (DFB) lasers are one of the most commonly used transmitters for high bit rate and long-haul fibre-optic communication DWDM systems nowadays. However, the relative high cost of the DFB lasers is a significant barrier of the development in fibre-optic communication techniques for more cost-sensitive applications such as fibre-to-home access and short-reach optical interconnects. As a result, the more economical Fabry-Perot (FP) multimode laser diodes can be a very competitive replacement.

Contrarily to their price advantage, the multimode laser diodes have some systematical performance imperfections to overcome; for instance, the dispersive broadening, mode partition noise and frequency chirping.

Frequency chirping is not a significant issue in a 1.33-μm laser diode system.

The dispersion broadening is caused by the dispersive nature of optic fibre. The photon stream emitted by FP lasers are in multi wavelength, which have different group velocity thus different group velocity delay (GVD) through the fibre link. As a result, the received spectral width will be broadened, which causes intersymbol interference. However, it has been shown that the use of single mode fiber can nearly avoid the intermodal dispersion problem (Agrawal, 2002, p203). Mode partition noise is an important factor especially in a single-mode fibre system. It is caused by instantaneous power redistribution among laser longitudinal modes and the different group delay of longitudinal modes due to fibre's chromatic dispersion nature. Since this noise is function of laser power distribution spectrum and fibre dispersion, once the bit error rate (BER) reaches the floor, the system signal-to-noise ratio (SNR) becomes independent of input signal power.

In Chapter 2, a set of coupled differential equations will be derived to describe the physical nature of energy transfer between photons and carriers in a multimode laser diode. In order to better understand the reactive behaviour of the multimode laser diode, the two coupled multimode rate equations are numerically solved without adding noise. The resulting illustration of output photon and carrier fluctuation will be employed to analyze the transient response of a multimode laser diode under two different scenarios: static and dynamic analysis.

As a continuity and extension of Chapter 2, the following chapter will bring Langevin noise terms into the coupled rate equations. The transient response of photon and carrier numbers is plotted under the noise circumstance, and it will be compared with which without noise. At the same time, in Chapter 3 a analytical expression of MPN power penalty is developed, which also is a verification of the

validity of the numerical model.

In order to give a better direct view of MPN effects, a numerical model of a fiber-optic communication system will be constructed in Chapter 4. The entire fibre-optic system consists of a multimode laser diode, a single mode fibre and a PIN photodiode. The system performance is described in terms of BER, Q factor, and eye diagram. In addition, Chapter 4 will also provide supplementary solutions to problems of system performance degradation.

Chapter 2

Multimode Rate Equations

2.1 Background

In a simple two level atomic system, there are three major activities related to photon emission rate, which are absorption, stimulated emission and spontaneous emission.

An incoming photon can exhaust its energy by pumping up an electron in the valence band (lower energy level) to the conduction band (higher energy level), and this process is called absorption. Figure 2.1 shows the absorption process as follow.

As shown in Figure 2.2, in a stimulated emission process, an incident photon can stimulate an electron in the higher energy level to relax in the lower energy level and emit another photon.

Contrarily, in spontaneous emission a photon is emitted by undergoing a transition to the lower energy level without stimulation. Figure 2.3 illustrates this process shown as below.

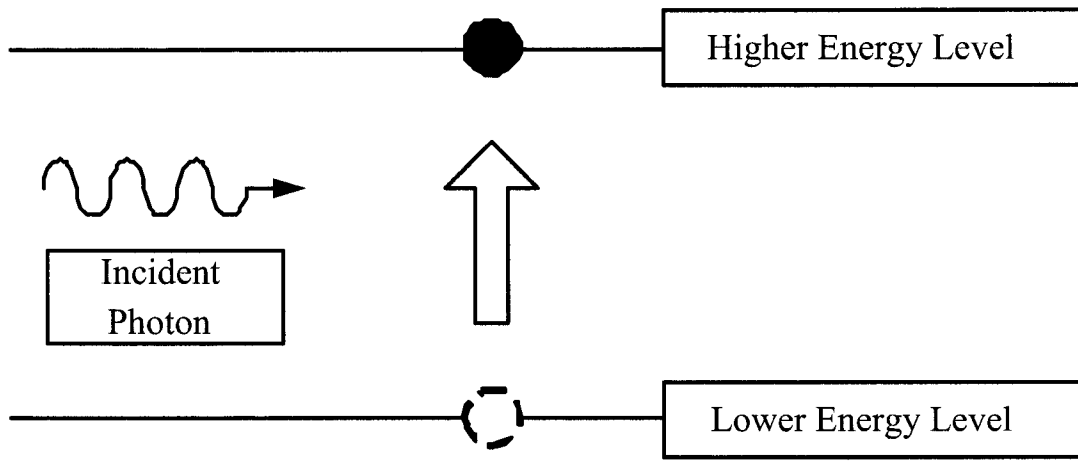

Figure 2.1: Absorption process of a two level atomic system

With the understanding of the above three processes, the laser rate equation can be described in a general form of ([9])

$$\left(\frac{dN}{dt}\right)_{Total} = \left(\frac{dN}{dt}\right)_{Inj} + \left(\frac{dN}{dt}\right)_{Stim} + \left(\frac{dN}{dt}\right)_{Spon} + \left(\frac{dN}{dt}\right)_{NR} \quad (2.1)$$

$$\left(\frac{dS}{dt}\right)_{Total} = \left(\frac{dS}{dt}\right)_{Loss} + \left(\frac{dS}{dt}\right)_{Stim} + \left(\frac{dS}{dt}\right)_{Spon} \quad (2.2)$$

where S and N stands for photon and carrier density. The physical meaning of each term in Equation 2.1 and 2.2 is defined as:

$\left(\frac{dN}{dt}\right)_{Inj} = \frac{J}{qd}$ is carrier gain due to injected (input) current. J is current density, unit charge $q = 1.602176487 \times 10^{19}$ C, and d is the thickness of laser active region;

$\left(\frac{dN}{dt}\right)_{Stim} = -GS$ is the carrier loss due to stimulated emission;

$\left(\frac{dN}{dt}\right)_{Spon}$ is carrier loss due to spontaneous emission;

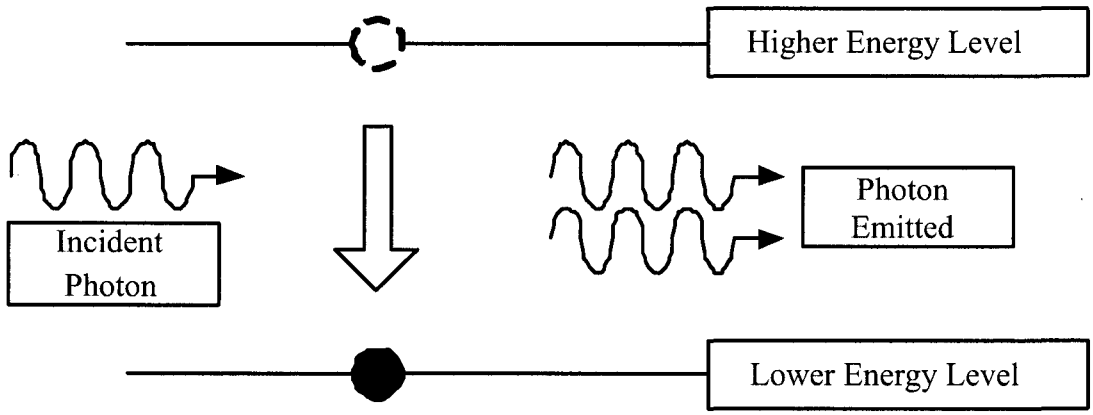

Figure 2.2: Stimulated emission process of a two level atomic system

$\left(\frac{dN}{dt}\right)_{NR}$ is the carrier loss due to non-radiative emission;

$\left(\frac{dS}{dt}\right)_{Loss} = -\frac{S}{\tau_{sp}}$ represents loss due to photon decay, where $\tau_{sp}$is the spontaneous emission lifetime of electrons;

$\left(\frac{dS}{dt}\right)_{Stim} = GS$ is correspondingly photon gain due to stimulated emission. G is the gain coefficient, which will be further derived in multimode laser rate equation;

$\left(\frac{dS}{dt}\right)_{Spon} = R_{sp}$ is photon gain due to spontaneous emission.

As a summary, Equation 2.1 and 2.2 can be expanded as follows,

$$\left(\frac{dN}{dt}\right)_{Total} = \frac{J}{qd} - GS - \frac{N}{\tau_{sp}} \tag{2.3}$$

$$\left(\frac{dS}{dt}\right)_{Total} = GS - \frac{S}{\tau_{sp}} + R_{sp} \tag{2.4}$$

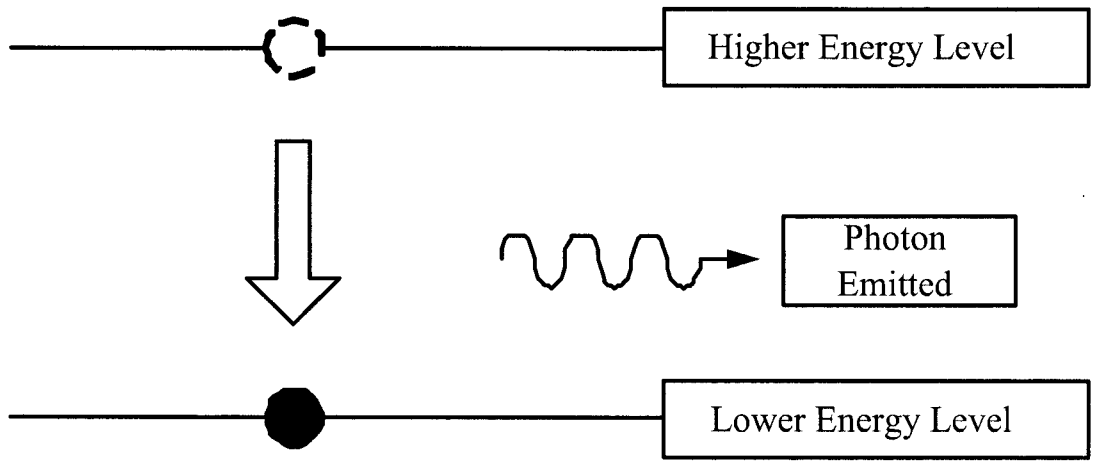

Figure 2.3: Spontaneous emission process of a two level atomic system

2.2 Multimode Laser Diode Rate Equation

The energy interchange between photons and carriers in multimode laser diode can be described by absorption, spontaneous and stimulated emission, which is governed by a set of coupled nonlinear differential equations in the general form of Equation 2.3 and 2.4 ([1] Marcuse, D. 1983). Some works have been done on the time dependent multimode laser rate equation modeling, and the carrier and photon number is given by ([1]-[2])

$$\left(\frac{dN}{dt}\right) = \frac{J}{qd} - \frac{N}{\tau_{sp}} - \frac{c}{\eta n_g}\sum_{m=1}^{M} g_m S_m \tag{2.5}$$

$$\left(\frac{dS_m}{dt}\right) = \frac{\gamma_m}{\tau_{sp}} D_m N + \frac{c}{n_g}\left(g_m - \alpha\right) S_m \tag{2.6}$$

by neglecting the nonlinear gain saturation, the gain coefficient of each mode is define as

$$g_m = \eta \frac{n_g}{c} A(D_m N - N_0) \tag{2.7}$$

The physical meaning of each parameter in Equation 2.6 - 2.7 is listed in Table 2.2.

Several parameters in Table 2.2 need to be further defined. Since only a small portion of spontaneous emission can be contributed to a given mode, a coefficient γ_m is introduced to determine the fraction accepted by m^{th} mode.

$$\gamma_m = \frac{\eta \lambda_m^2}{4\pi n_r^2 D d} \tag{2.8}$$

The photon loss is also caused by imperfect reflection of the laser cavity mirrors; therefore the effective loss coefficient is related to the reflectivity and length of laser cavity, which is defined as,

$$\alpha = \alpha_0 + \frac{1}{L} \ln(\frac{1}{R}) \tag{2.9}$$

The stimulated emission factor A is defined as

$$A = \frac{\gamma_m}{\eta \tau_{sp}} DL \frac{d}{\eta} \tag{2.10}$$

The mode distribution line shape factor D_m determines the shape of the power distribution over the multi lasing wavelengths. It is usually assumed to be Gaussian or Lorentzian distribution. The Lorentzian distribution function is applied here, and it is given by,

Parameter	Symbol	Typical Value	Unit
Carrier Density	N	-	m^{-3}
Photon Density of m^{th} Mode	S_m	-	m^{-3}
Time Coordinate	t	-	s
Injected Current Density	J	-	$A{\cdot}m^{-3}$
Unit Electron Charge	q	$1.602176487{\times}10^{19}$	C
Thickness of Active Laser Region	d	0.3	μm
Width of Laser Stripe	D	5	μm
Length of Laser Cavity	L	250	μm
Spontaneous Emission Carrier Lifetime	τ_{sp}	$3{\times}10^{-9}$	s
Speed of Light	c	$3{\times}10^{8}$	m/s
Group Index of Laser Medium	n_g	4	-
Refractive Index of Laser Medium	n_r	3.4	-
Mode Confinement Factor	η	0.5	-
Gain Coefficient of m^{th} Mode	g_m	-	Refer to 2.7
Effective Cavity Loss Coefficient	α	-	Refer to 2.9
Reflectivity of Cavity Mirrors	R	0.3	-
Carrier Number Threshold	N_0	8.25×10^5	m^{-3}
Loss Coefficient	α_0	2000	m^{-1}
Spontaneous Emission Factor of m^{th} Mode	γ_m	-	Refer to 2.8
Line Shape Factor of Mode Distribution	D_m	-	Refer to 2.11
Stimulated Emission Factor	A	-	Refer to 2.10
Lasing Wavelength at the Peak of Distribution (Central Wavelength)	λ_0	1310	nm
Lasing Wavelength of m^{th} mode	λ_m	-	nm
Wavelength Spacing Between Two Adjacent Mode	$\Delta\lambda_c$	0.845	nm
Effective Gain Spectral Linewidth Parameter	$\Delta\lambda_D$	60	nm

Table 2.1: Definitions and typical values of the rate equation parameters

$$D_m = \frac{\frac{\Delta\lambda_c}{\pi\Delta\lambda_D}}{1+\left(\frac{\lambda_m-\lambda_0}{\Delta\lambda_D}\right)^2} \tag{2.11}$$

2.3 Modulation Response

The multimode semiconductor laser diode will be directly modulated by an input driving current. In the absence of noise, the transient response of laser diode is dependent of this injection current density J. Under direct modulation scheme, J is time dependent, which consists of two parts: a bias current level J_b and a periodically varying waveform $J_m(t)$ which carries information. The total injection current density can be written as

$$J(t) = J_b + J_m(t) \tag{2.12}$$

In digital communication, two electric levels are used to represent '0' and '1'. In order to avoid the complete turn-off of the laser diode while transmitting 0s, the bias current J_b is assumed to be about 10% above the threshold current J_{th}. The parameter determining the relation of J_b and J_m amplitude is called modulation depth, which is defined as

$$m = \frac{[J_m(t)]_{max}}{J_b - J_{th}} \tag{2.13}$$

The modulation response will be mainly discussed in two sections, Static Analysis and Dynamic Analysis [4]. All simulation results are generated with m=17 modes and with other parameter values listed in Table 2.2.

2.3.1 Static Analysis

The DC analysis describes steady state characteristics of the multimode rate equations, by setting the time derivatives of Equation 2.6 and 2.6 equal to zero. The steady state photon and electron density are found to be

$$\overline{N} = \tau_{sp}\left[\frac{J}{qd} - \frac{c}{\eta n_g}\sum_{m=1}^{M} g_m S_m\right] \tag{2.14}$$

$$\overline{S}_m = -\frac{\gamma_m D_m n_g}{c\tau_{sp}(g_m - \alpha)}\overline{N} \tag{2.15}$$

The calculation for steady state photon and electron density is useful to feature a general interest in characterizing laser performance, which is called the Light-Current curve (L-I curve) ([4] Agrawal, G. P., p239). The L-I curve shows how the total output power varies corresponding to injected power.

As illustrated in the Figure 2.4 L-I curve, the output power remains in a very low level until the injected current reaches its threshold. In this case, $I_{th} \approx 10.1mA$. And beyond this point, output optical power increases linearly with respect to the injected current.

2.3.2 Dynamic Analysis

The dynamic response of emitting photon rate is similar to a relaxation oscillation, which goes up to an overshoot, fluctuates at high frequencies within certain time duration and then relaxes at a steady state level. The steady state behaviour has been discussed peviously, and this section mainly focuses on the oscillation aspect.

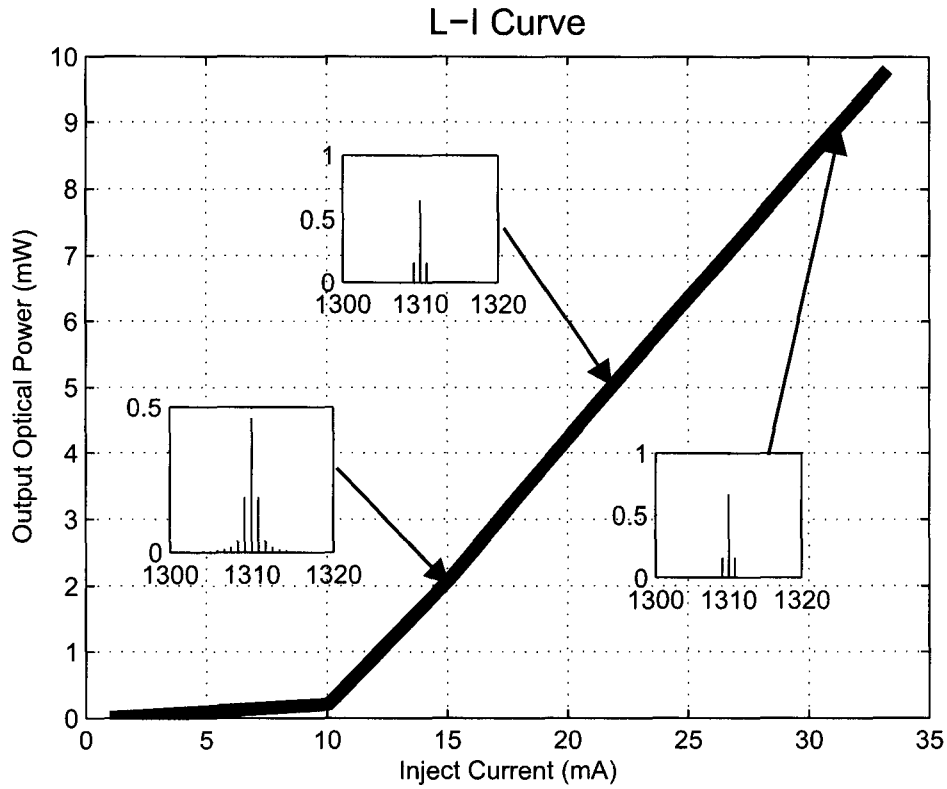

Figure 2.4: L-I curve for total output power

In dynamic analysis, two different scenarios will be set with the help of evaluating modulation depth m. When $m \ll 1$, which means the amplitude of $J_m(t)$ is greatly smaller than J_b, the oscillation of the current is small enough so that the nonlinear effect caused by deviations between photon/carrier fluctuations and average level can be neglected. And the second case is based on the condition of $m \gg 1$.

To precede numerical simulation, the modulation current density function is defined as Gaussian, which is given by

$$J_m(t) = J_b + J_0\left(1 - e^{-\left(\frac{t}{t_r}\right)^2}\right) - J_0 \cdot e^{-\left(\frac{t-T}{t_r}\right)^2} \tag{2.16}$$

The parameters appearing in Equation 2.16 are provided with their values in Table 2.3.2,

Parameter	Value
J_{th}	$0.807kA/cm^2$
J_b	$11 \cdot J_{th}$
J_0	$0.1 \cdot J_{th}$
m	0.01
T	$5ns$
t	$0.1ns$

Table 2.2: Injection current density components and their values for dynamic analysis when $m \ll 1$

The injection current is shown in Figure 2.5 for a single bit period of '1' with Bell curve shaped edges.

The simulation results of photon number S and carrier number N within one bit period under small signal analysis are illustrated in Figure 2.6 and 2.7 below. To see the details of the fluctuation portion, it is zoomed in to be within 2ns in Figure 2.6, in which the solid line is carrier number response and dashed line represents total photon fluctuations.

Figure 2.7 specifies photon response of the main and first three side modes, in which the power of side modes are quite competitive with main mode, and as they relax on steady state the main mode power becomes to dominate. This behaviour is consistent with the LI curve with power distribution spectrums shown in Figure 2.4.

Although the dynamic analysis for $m \ll 1$ is useful for predicting parameter

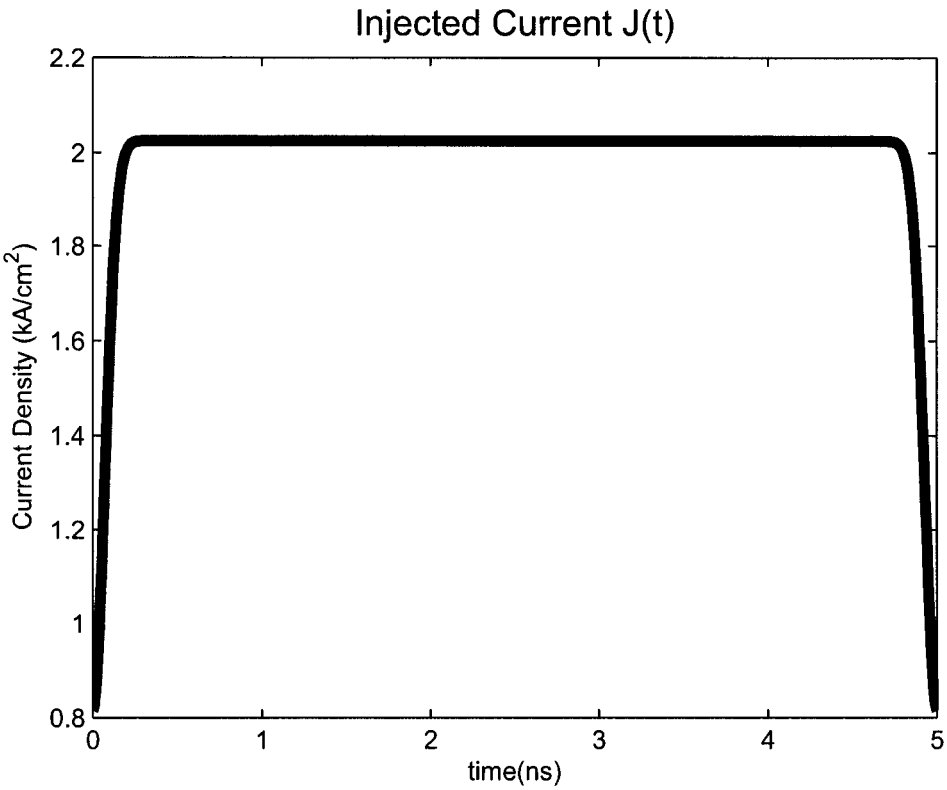

Figure 2.5: A single period of injected current representing a bit '1'

dependence, it is not usually valid under practical conditions [4]. In optical communication systems, the bias current density is usually set slightly above or close to threshold, and the modulation depth m will no longer satisfy the prior criterion. As a result, the nonlinear effects caused by large periodical oscillation of injection current can not be neglected, and the second scenario of $m \gg 1$ becomes a necessity to simulate the real life case. The numerical modeling is generated with the same period and rise time, and other parameters are assigned in Table 2.3.2.

Figure 2.8 shows carrier number N and photon numbers S for the transient response with a bit rate of 0.2Gb/s. Solid line is carrier number and dashed line

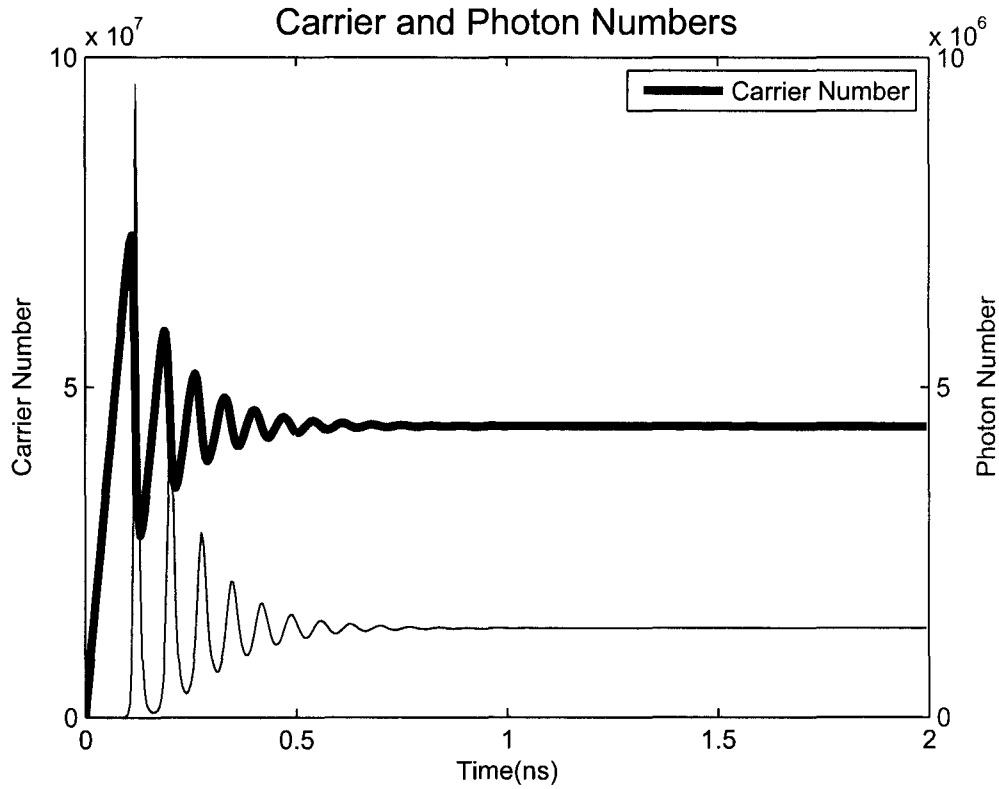

Figure 2.6: Carrier and photon numbers under such condition that $m = 0.01$, with $J_0 = 0.1 \cdot J_{th}$ and $J_b = 11 \cdot J_{th}$

represents photon number.

Figure 2.9 gives a detailed description of main and side modes of photon numbers within a single period time.

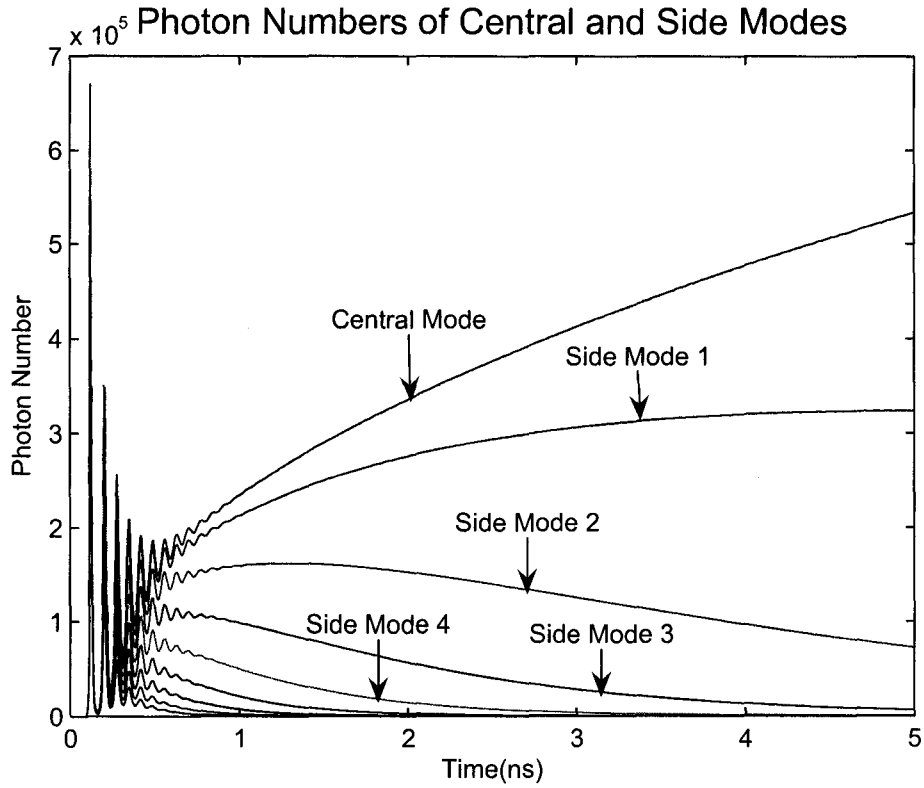

Figure 2.7: Photons numbers for main mode and another 3 side modes when modulation depth $m = 0.01$, with $J_0 = 0.1 \cdot J_{th}$ and $J_b = 11 \cdot J_{th}$

Parameter	Value
J_{th}	$0.807kA/cm^2$
J_b	$1.01 \cdot J_{th}$
J_0	$1.5 \cdot J_{th}$
m	150
T	$5ns$
t	$0.1ns$

Table 2.3: Injection current density components and their values when $m \gg 1$

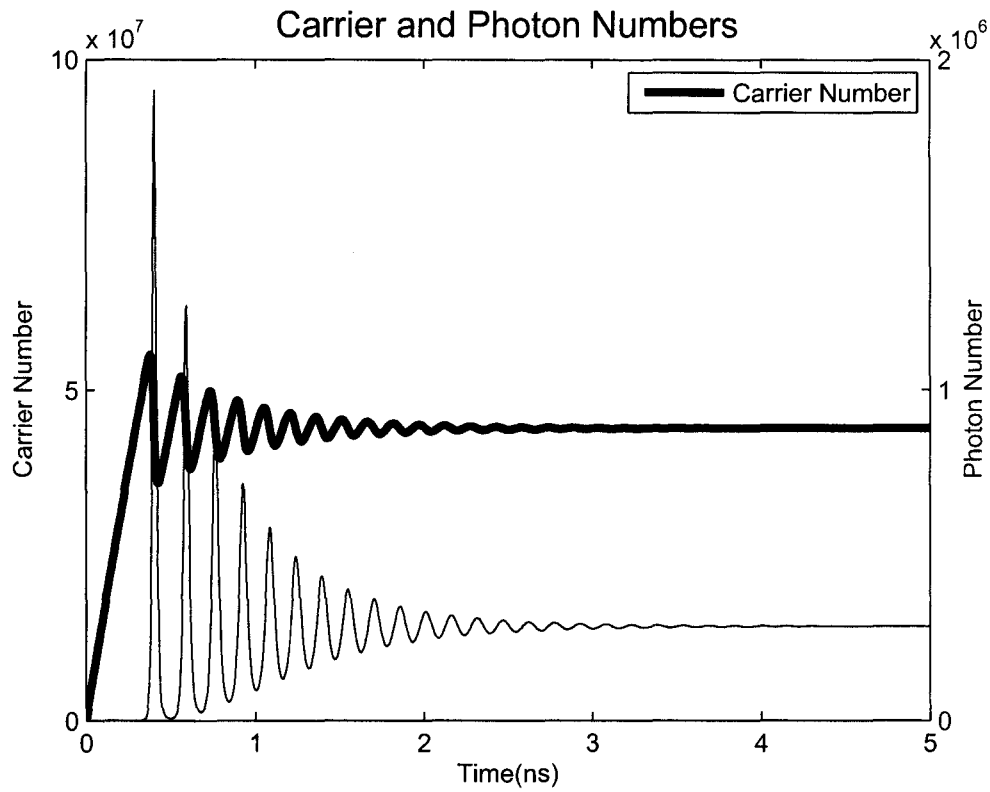

Figure 2.8: Carrier and photon numbers under such condition that $m = 150$, with $J_0 = 1.01 \cdot J_{th}$ and $J_b = 1.5 \cdot J_{th}$

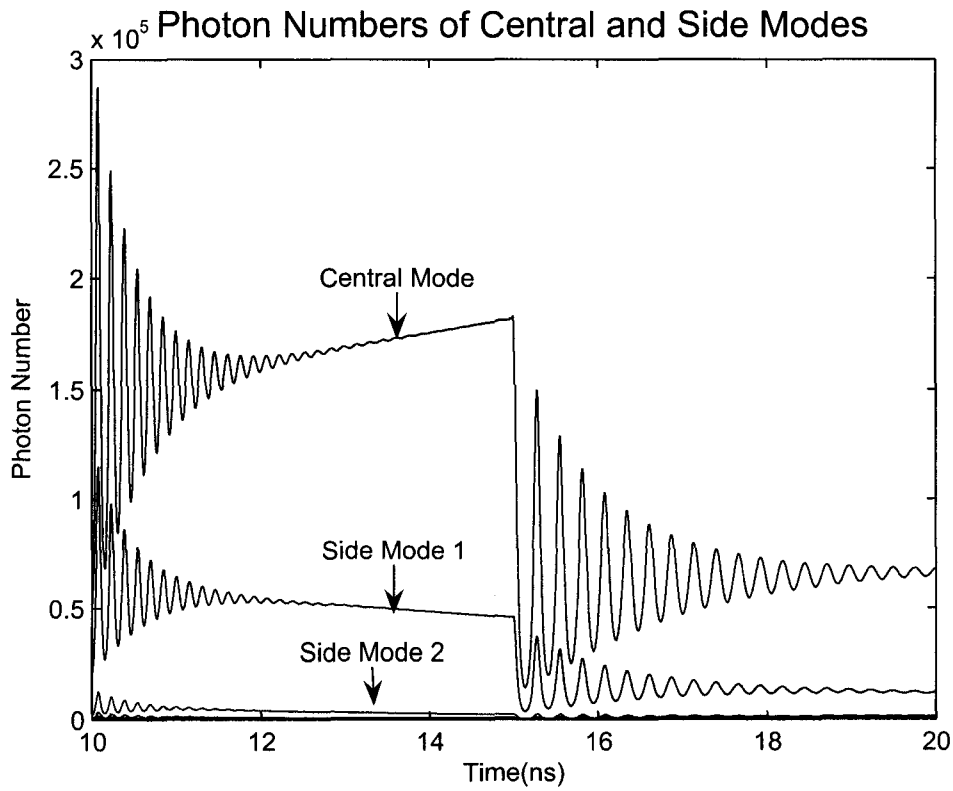

Figure 2.9: Photons numbers for main mode and another 3 side modes when modulation depth $m = 150$, with $J_0 = 1.01 \cdot J_{th}$ and $J_b = 1.5 \cdot J_{th}$

Chapter 3

Noise Driven Rate Equations

The rate equation model constructed in Chapter 2 is commonly used to study the dynamics of photon and carrier populations in multimode lasers. They are sufficient for predicting the average photon and carrier transient response behaviours and relaxation oscillation. However, their deficiency in statistical photon fluctuation limits the function of describing stochastic power shifting from main mode to other side modes. If zoomed in on picosecond scale, the output contains a large number of random fluctuations. Therefore, with the direct modulation scheme applied the resulting output will perform such fluctuations that "could introduce substantial errors in a communication system" ([2]).

In order to comprehensively study the behaviours of multimode lasers, the noise driven rate equations were introduced in some literatures [1]-[3]. In the first section, a numerical model of noise driven multimode rate equation will be built based on review of Marcuse's theory ([2]), and the simulation results of transient response will be compared with non noise-driven rate equation model. Followed by a theoretical derivation of power penalty caused by MPN in the second section,

the validation of simulation results will be qualified. As a summary, the simulation results and comparison are provided in the last section.

3.1 Noise Driven Rate Equations

Similar to the rate equations without noise derived in the previous chapter, according to Marcuse ([2]), the noise function can be directly added to the photon and carrier number differential equations, which become to be as follows

$$\frac{dN}{dt} = \frac{J}{qd} - \frac{N}{\tau_{sp}} - \frac{c}{\eta n_g}\sum_{m=1}^{M} g_m S_m + F_N(t) \tag{3.1}$$

$$\frac{dS_m}{dt} = \frac{\gamma_m}{\tau_{sp}} D_m N + \frac{c}{n_g}\left(g_m - \alpha\right) S_m + F_m(t) \tag{3.2}$$

In order to make it consistent with previous sections, the noise driven rate equation employed here are slightly modified by replacing photon and carrier density (used in [2]) with photon and carrier number. The physical meanings and typical values of parameter used in Equation 3.2 and 3.2 are consistent with those in Table 2.2.

The random noise source terms $F_N(t)$ and $F_m(t)$ are assumed to be Gaussian distribution, and the autocorrelation and cross correlation functions of $F_N(t)$ and $F_m(t)$ are proportional to Dirac delta functions ([2]),

$$\langle F_N(t)F_N(t')\rangle = V_N^2\delta(t-t') \tag{3.3}$$

$$\langle F_m(t)F_p(t')\rangle = V_m^2\delta_{mp}\delta(t-t') \tag{3.4}$$

$$\langle F_N(t)F_m(t')\rangle = r_m V_N V_m\delta(t-t') \tag{3.5}$$

where V_N^2 and V_m^2 are the variance of $F_N(t)$ and $F_m(t)$, and r_m is the correlation coefficient. The variance V_N^2 and V_m^2 are derived from laser Langevin equations. The calculation has been done in Marcuse's work, and the results are directly applied here,

$$V_N^2 = \frac{J}{qd} + \frac{N}{\tau_{sp}} + \frac{c}{\eta n_g}\sum_{m=1}^{M} g_m^+ S_m \tag{3.6}$$

$$V_m^2 = \frac{\gamma_m}{\tau_{sp}} D_m N + \frac{c}{n_g}\left(g_m^+ + d^{-1}\right) S_m \tag{3.7}$$

$$r_m V_N V_m = -\left(\frac{n_g\gamma_m}{c\tau_{sp}}\left(D_m N + N_0\right)\right) \tag{3.8}$$

with the gain compression factor

$$g_m^+ = \frac{n_g\gamma_m}{c\tau_{sp}}\left(D_m N + N_0\right) \tag{3.9}$$

It is easy to notice that Equation 3.7 and 3.8 share a high similarity with noise driven rate equations, and it can be understood in such a way that process "such as absorption or emission of photon or insertion or removal of carrier into or from upper energy level becomes a source of shot noise".

Now if noise source terms can be expressed in terms of their variances, the

noise driven rate equation can be modeled by solving an additional set of differential equations. If only a discrete time interval is considered, Equation 3.4 can be expressed as

$$\langle F_N(t)F_N(t')\rangle = \begin{cases} \frac{1}{\Delta t}V_N^2 & \text{for } |t-t'| \leq \Delta t \\ 0 & \text{else} \end{cases} \tag{3.10}$$

Therefore, the stochastic function $F_N(t)$ can be written as

$$F_N = \frac{V_N}{\sqrt{\Delta t}}x_N \tag{3.11}$$

where x_N is a random variable with Gaussian distribution and $x_N = \pm\sqrt{2}erf^{-1}(u)$ for $0 < u < 1$. The sign of x is randomly chosen, and the inverse error function $erf^{-1}(u)$ can be easily generated in MATLAB environment with command "erfinv(u)".

Marcuse's work also provided the expression of $F_m(t)$, which is

$$F_m = r_m\frac{V_m}{V_N}F_N + \frac{V_m}{\sqrt{\Delta t}}\sqrt{1-r_m^2}x_m \tag{3.12}$$

where x_m can be generated in the same way as x_N.

The simulation is run with the same basic parameter values used in Table 2.2. The results are shown in Figure 3.1 and 3.2. The injection current is biased under dynamic condition with modulation depth equal to 1, i.e. the pulse oscillation is comparable with offset level. It is apparent that even at the steady state a small deviation still fluctuates randomly above and below the average level.

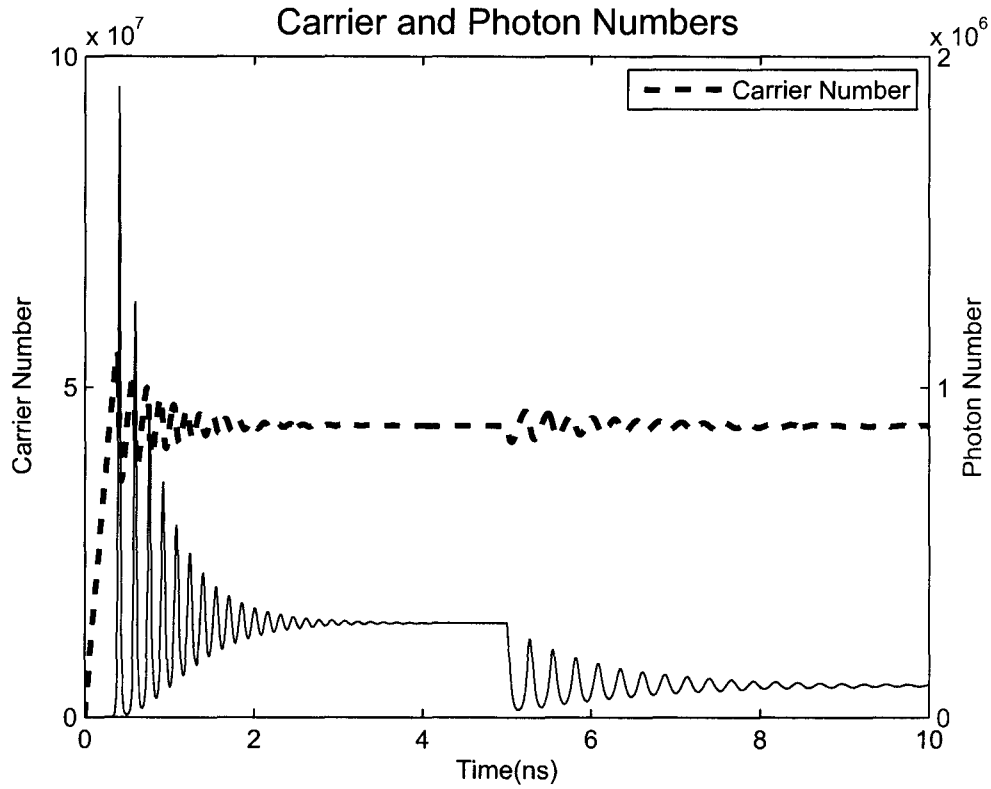

Figure 3.1: Noise driven photon and carrier responses

In Figure 3.1, solid and dashed line represents carrier and photon response correspondingly. The first turn-on rises up a steep spine, and it becomes smoother throughout the bit sequence. The carrier and photon population oscillates on a similar level to Figure 2.8 and 2.9, and the only difference is the petit fluctuations on the tail of each bit.

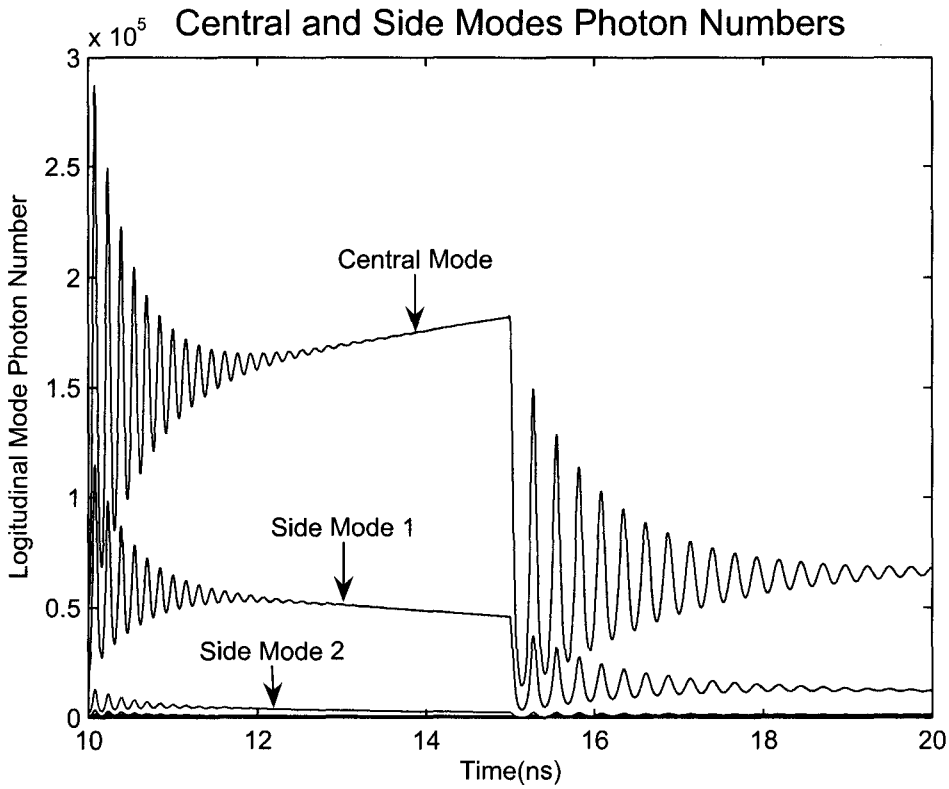

Figure 3.2: Noise driven photon fluctuation of the main mode and first three side modes

3.2 MPN and its Power Penalty

It has been shown previously that mode partition noise has significant effects on achievable transmission distance of a fiber optic link [5]. The mode partition noise is mainly due to dispersive nature of optical fiber and power redistribution among different longitudinal modes [6].

Dispersion in optical fiber or the broadening effect can lead to intersymbol interference, which technically reduces maximum achievable bit rate. However, this

can be compensated by increasing the launched power to laser diode so that the required signal-to-noise ratio (SNR) will be reached. In average, the power spectrum is distributed in a Gaussian shape with the main mode power at the wavelength spectral centre. In reality, however, photon fluctuations at different wavelengths start to oscillation randomly. When one or more side modes dominate the total power, linewidth broadening and central wavelength shifting will occur and the output optic signal will be distorted with certain power penalty.

In contrary, once a bit error rate floor is observed, SNR degradation caused by power redistribution can not be balanced out by increasing launched power. The mode partition noise model widely used nowadays was first developed by Ogawa [7]. This theory is approximately accurate under such conditions:

1. The total power of each optic pulse must remain constant. If total number of N modes are emitted, A_i is the amplitude of i_{th} longitudinal mode of the multimode laser diode. By normalizing with respect to the total power, A_i must satisfy:

$$\sum_{i=1}^{N} A_i = 1 \tag{3.13}$$

2. The time averaged power distribution spectrum is defined as:

$$\overline{A}_i = p(\lambda_i) = \int \cdots \int A_i p(A_1, A_2, ..., A_N) dA_1 dA_2 \cdots dA_N, for any i \tag{3.14}$$

3. The received pulse waveform of i_{th} mode is denoted by $f(\lambda_i, t)$, and due to different fiber dispersion on different wavelength, each mode will have different delay at the receiver end. Therefore, the total received signal is the

sum of each pulse multiplied by its power distribution weight.

$$r(t) = \sum_{i=1}^{N} f(\lambda_i, t) A_i \tag{3.15}$$

At each sampling time $t = t_0$, the MPN variance is evaluated as $\sigma^2_{MPN} = \overline{r^2(t_0)} - \overline{r(t_0)}^2$. By substituting Equation 3.14 and 3.15 into it, we get

$$\begin{aligned} \sigma^2_{MPN} &= \sum_i f^2(\lambda_i, t_0)\overline{A_i^2} + 2\sum_i \sum_j f(\lambda_i, t_0) f(\lambda_j, t_0)\overline{A_i A_j} \\ &\quad - \sum_i f^2(\lambda_i, t_0)\overline{A_i}^2 - 2\sum_i \sum_j f(\lambda_i, t_0) f(\lambda_j, t_0)\overline{A_i}\ \overline{A_j} \end{aligned} \tag{3.16}$$

Since from Equation 3.14 we know that

$$\begin{aligned} \overline{A_i A_j} &= \int A_i A_j p\left(A_1, A_2, \cdots A_N\right) dA_1 dA_2 \cdots dA_N \\ \overline{A_i} &= \int A_i p\left(A_1, A_2, \cdots A_N\right) dA_1 dA_2 \cdots dA_N \\ \overline{A_i^2} &= \overline{A_i\left(1 - \sum_{j \neq i} A_j\right)} = A_i - \sum_{j \neq i} \overline{A_i A_j} \end{aligned}$$

Therefore, by substituting the above three equations into Equation 3.16 the fluctuation variance can be rewritten as follows:

$$\sigma^2_{MPN} = k^2 \left[\sum_i f^2(\lambda_i, t_0)\overline{A_i} - \left(\sum_i f(\lambda_i, t_0)\overline{A_i}\right)^2\right] \tag{3.17}$$

where k is introduced here as mode partition coefficient, which is defined as

$$k^2 = \frac{\overline{A_i^2} - \overline{A_i}^2}{\overline{A_i} - \overline{A_i}^2} \tag{3.18}$$

From [5] the power penalty due to mode partitioning is given by

$$\alpha_{MPN} = 5 \log \left(\frac{1}{1 - Q^2 \sigma_{MPN}^2} \right) \tag{3.19}$$

The value of Q is determined by the system required bit error rate, which is defined as

$$BER = \frac{1}{Q\sqrt{2\pi}} e^{\left(-\frac{Q^2}{2}\right)} \tag{3.20}$$

Some commonly used BER values and their corresponding Q factors are calculated by using Equation 3.20 and their relation is plotted in Figure 3.3. Some commonly used BER and Q factors are also provided in Table 3.2 for convenience.

Q	BER
6.002	10^{-9}
6.345	10^{-10}
6.709	10^{-11}
7.037	10^{-12}

Table 3.1: List of some useful BER and its corresponding Q factors

Equation 3.17 is useful for both analytical and numerical solution of MPN power penalty. Once they are derived and simulated under certain circumstances, it will be easier to tell if the analytical method is optimistic or pessimistic.

The analytical calculation can be derived from a predetermined specific received signal waveform $f(\lambda_i, t_0)$ and the power distribution spectrum $\overline{A_i}$. Several necessary assumptions are made at this point.

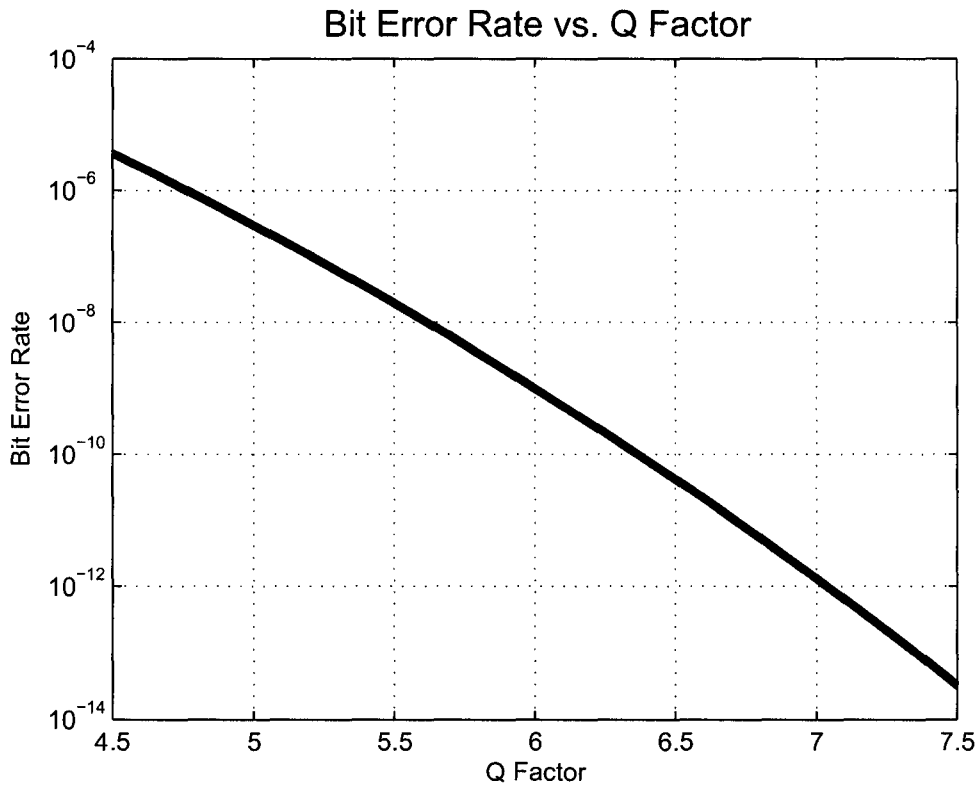

Figure 3.3: Plot of Q factor and its corresponding bit error rate

It is assumed that the steady state power distribution spectrum $\overline{A_i}$ is Gaussian, which is given by,

$$\overline{A_i} = \frac{1}{\sigma\sqrt{2\pi}} e^{\left[-\frac{(\lambda_i-\lambda_0)}{2\sigma^2}\right]^2} \tag{3.21}$$

A trick need to be played on the choice of the received signal waveform. If a cosine shaped waveform shown in Figure 3.4 is transmitted through a segment of fibre with certain dispersion, the received signal will remain the same shape but with a delay in time coordinate ΔT. Due to the multi wavelength nature of FP

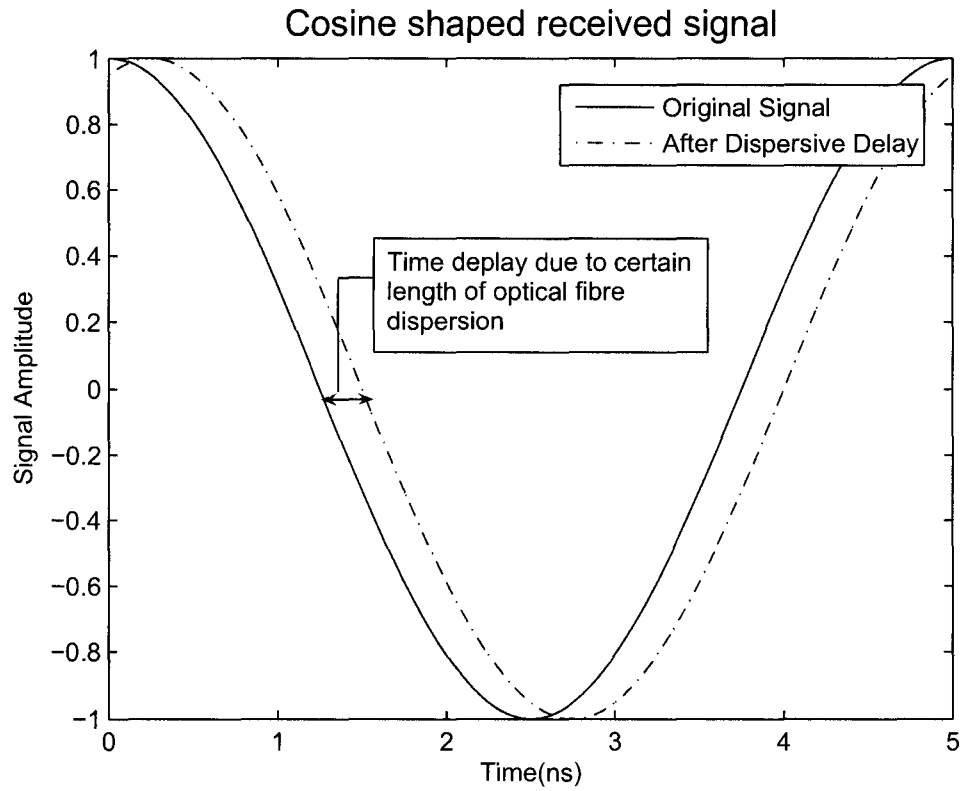

Figure 3.4: Cosine shaped waveform and received signal after certain length of optical fibre dispersion

lasers, different longitudinal modes propagate through the fibre link at different speeds, therefore they will reach at the receiver side with different time delay. As a result, the eye diagram pattern will be fuzzy, and at the sampling point the receiver will have a higher possibility to make a wrong decision on 0s or 1s. This is the so-called intersymbol interference. However, the silver lining is that this situation has been solved in digital communication by adding a raised cosine shaped equalizer.

Consequently, for the purpose of optimizing system performance, the received signal waveform is assumed to be cosine,

$$f_i(\lambda_i, t_0) = \cos\left[\pi B\left(t_0 + \Delta T\right)\right]$$

where ΔT is the time delay of each mode due to certain length of fiber with dispersion coefficient D, and it is given by

$$\Delta T = LD\left(\lambda_i - \lambda_0\right)$$

The sampling circuit takes value at every t_0 second, so that the received signal function can be rewritten as

$$f_i(\lambda_i, t_0) = \cos\left[\pi BLD\left(\lambda_i - \lambda_0\right)\right] \tag{3.22}$$

To simplify the calculation in Equation 3.17, the discrete sum will be approximated as integral, and the final result can be reached as

$$\sigma_{MPN} = \frac{k}{\sqrt{2}}\left[1 - e^{(-\pi BLD\sigma)^2}\right] \tag{3.23}$$

Therefore, the power penalty is found by substituting Equation 3.23 into 3.19, which is rearranged as,

$$\alpha_{MPN} = 5\log\left(\frac{1}{1 - \frac{k^2Q^2}{2}\left[1 - e^{(-\pi BLD\sigma)^2}\right]}\right) \tag{3.24}$$

The formula derived above for calculating the power penalty is under such two conditions that the input waveform is cosine and the power distribution spectrum is Gaussian. Although the assumptions do not always hold in reality, it is still valid as an approximation for comparison purpose.

Parameter	Symbol	Average	Range
Fiber Length	L	$40km$	-
Bit Rate	B	$1.7Gbit/s$	-
Dispersion	D	$0.102ps/km/nm^2$	-
Spectral Width	σ	$2.0nm$	$\pm 0.25nm$
Bit Error Rate	BER	10^{-9}	-
MPN Coefficient	k	0.5	0.5-0.7
Wavelength Window Width	$\lambda_i - \lambda_0$	1310nm	$\pm 5nm$

Table 3.2: Parameters and values for calculating power penalty due to MPN

The numerical method of calculating MPN power penalty will be described in Chapter 4, and its results will be compared with those evaluated by analytical solution.

3.3 Simulation Results

The power penalty due to MPN is calculated using Equation 3.24, and the parameters are given in Table 3.3.

In Figure 3.5, the MPN power penalty versus wavelength is illustrated for k = 0.5. At the central lasing wavelength 1310nm, MPN power penalty is at minimum level of about 0.1dB, and as expanded to the side modes, the power penalty increases dramatically.

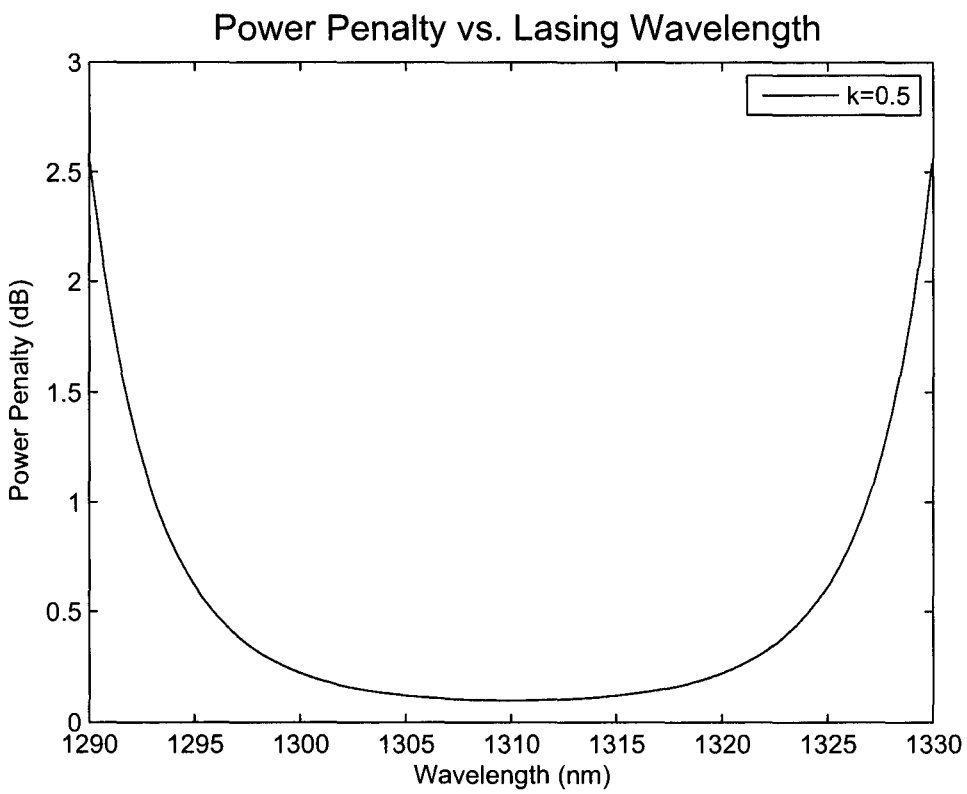

Figure 3.5: Plot of MPN power penalty versus lasing wavelength

Chapter 4

System Performance

As stated in Chapter 3, mode partitioning effects are significantly dependent of the dispersive nature of optic fibre. Therefore, without modeling optical fibre in the system the discussion on mode partition noise is pointless. In addition, at the receiver side, photodiode introduces shot and thermal noise that need to be taken into account as well. As a result, in order to show the effects of mode partition noise on system performance, it is necessary to connect optical fibre and photo detector models with the multimode laser diode, so that measures of bit error rate (BER), Q factor and eye diagram can be directly illustrated.

Since the focus is still on multimode laser diode, the simulation system only consists of an FP laser diode, a simple single mode optic fibre and PIN photodiode model (shown in Figure 4.1). The output signal is analyzed in terms of plotting eye diagram and evaluating MPN power penalty.

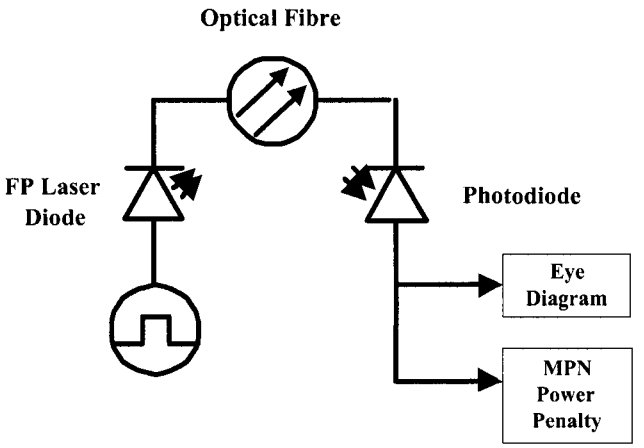

Figure 4.1: System Schematics

4.1 Optical Fibre

It is known that the single mode optical fibre can greatly reduces intermodal dispersive broadening caused by multi wavelength operation [15], the derivation of mathematical model is based on ECE756 course notes by Dr. Kumar [9].

The output waveform of laser diode is assumed to be a continuous wave $\varphi(x, y)$, and optic field distribution for a single wavelength after passing through a fibre with a length L on z coordinate is given by,

$$E(x, y, z, t) = \varphi(x, y)A(\omega)e^{-j\omega t + j\beta(\omega)z} \tag{4.1}$$

Since the laser diode with multi lasing wavelength is used, the total field distribution is the superposition of which due to a single wavelength,

$$E(x, y, z, t) = \varphi(x, y)\sum_{i=1}^{N} A(\omega)e^{-j\omega_i t + j\beta(\omega_i)z} \tag{4.2}$$

To simplify the calculation, the sum is approximated as integration, and Equation 4.2 becomes

$$\begin{aligned} E(x,y,z,t) &= \varphi(x,y)F(t,z) \\ F(t,z) &= \int_{-\infty}^{+\infty} \widetilde{A}(\omega)e^{-j\omega t+j\beta(\omega)z}d(\omega) \end{aligned} \tag{4.3}$$

where $\widetilde{A}(\omega)$ is the Fourier Transform of pulse profile in frequency domain, and $\beta(\omega)$ is the propagation constant which is expanded according to Taylor's Rule,

$$\beta(\omega) = \beta_0 + \beta_1(\omega-\omega_0) + \frac{1}{2}\beta_2(\omega-\omega_0)^2 + \frac{1}{6}\beta_3(\omega-\omega_0)^3 + ... \tag{4.4}$$

In Equation 4.4, the inverse group velocity and dispersion coefficient denoted as β_1 and β_2 are the first and second degree derivatives at $\omega = \omega_0$. Now, substitute Equation 4.4 into 4.3, we can easily get

$$\begin{aligned} F(t,z) &= \int_{-\infty}^{+\infty} \widetilde{A}(\omega-\omega_0)e^{-j(\omega_0 t-\beta_0 z)+j\beta_1(\omega-\omega_0)+\frac{1}{2}j\beta_2(\omega-\omega_0)^2 z}e^{-j(\omega-\omega_0)t}d(\omega-\omega_0) \\ &= e^{-j(\omega_0 t-\beta_0 z)}\int_{-\infty}^{+\infty} \widetilde{A}(\omega-\omega_0)e^{-j\beta_1(\omega-\omega_0)z+\frac{1}{2}j\beta_2(\omega-\omega_0)^2 z}e^{-j(\omega-\omega_0)t}d(\omega-\omega_0) \\ &= e^{-j(\omega_0 t-\beta_0 z)}\int_{-\infty}^{+\infty} \widetilde{A}(\omega-\omega_0)H(\omega-\omega_0)e^{-j(\omega-\omega_0)t}d(\omega-\omega_0) \end{aligned}$$

Apparently the transfer function of optical fibre is given by

$$H(\Omega) = e^{-j\beta_1(\omega-\omega_0)z+\frac{1}{2}j\beta_2(\omega-\omega_0)^2 z} \tag{4.5}$$

where $\Omega = \omega - \omega_0$.

It is obvious that Equation 4.5 is a function of wavelength, and it is also dependent of fibre length z, inverse group velocity β_1 and dispersion coefficient β_2. β_1 will cause propagation delay which leads to intersymbol interference (ISI), and β_2 will mainly lead to pulse broadening. Figure 4.1 and 4.2 shows the effects of β_1 and β_2 with respect to an input Gaussian pulse. The fibre model is simulated based on fundamental parameters assigned in Table 4.1.

Parameter	**Symbol**	**Value**
Inverse Group Velocity	β_1	$16ps/km$
Dispersion Coefficient	β_2	$-21ps^2/km$
Fibre Length	z	$20km$
Full Width Half Maximum	FWHM	$0.2ns$

Table 4.1: Values of optic fibre parameters used in simulation

In Figure 4.2, with inverse group velocity $\beta_1 = 16\ ps/km$ and $\beta_2 = 0\ ps^2/km$, the output peak is delayed by 0.32ns with respect to input signal. Since $\beta_2 = 0$, the transfer function Equation 4.5 becomes $H(\omega) = e^{j\beta_1 \omega z}$, and the term $\Delta t = \beta_1 z$ is actually the time shift after a transmission distance z. Substitute the values from Table 4.1, and we can get $\Delta t = 0.32ns$, which is consistent with the reading from Figure 4.2 (The input peaks at $t = 0.3ns$, and reading $t = 3.321$, which gives a time difference of 0.321ns).

When discussing dispersion effects, an important definition of dispersion length must be introduced here. Given fixed dispersion coefficient and pulse width, for a Gaussian pulse the dispersion length, i.e. L_D, is given as

$$L_D = \frac{T_0^2}{|\beta_2|} \tag{4.6}$$

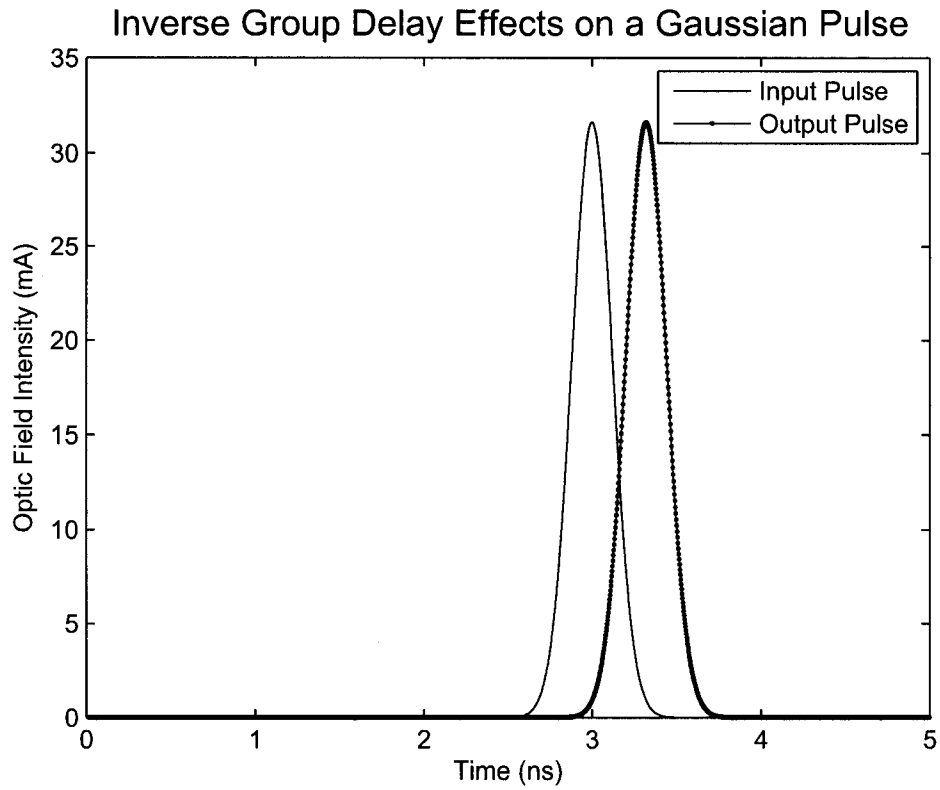

Figure 4.2: Group delay effect of a segment of optic fibre with $\beta_1 = 16\ ps/km$ and $\beta_2 = 0\ ps^2/km$

This means within the length L_D pulse propagating in the fibre can be received without broadening distortion. For example, with the parameter values provided in Table 4.1, the dispersion length is calculated to be 1144km. Thus, in the simulation of dispersion effects on a fibre length of 20km, the dispersion effects would be invisible. For a better view, Figure 4.3 is generated under such criteria that $\beta_2 = -2100\ ps^2/km$.

The analytical solution of the dispersion effects on a Gaussian pulse is straight forward. The input waveform is Gaussian, which is very helpful since its Fourier

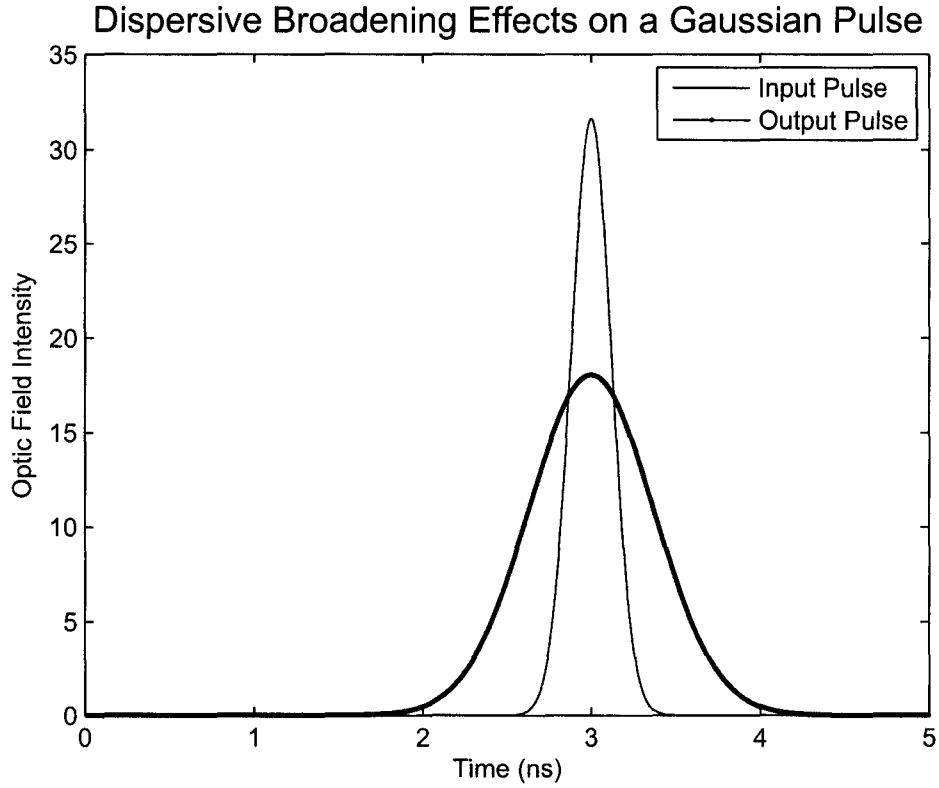

Figure 4.3: Group delay effect of a segment of optic fibre with $\beta_1 = 0\ ps/km$ and $\beta_2 = -2100\ ps^2/km$

transform is still in Gaussian shape but with slightly different coefficients. Let us assume the input signal is

$$S(0,T) = Ae^{\left(-\frac{T^2}{2T_0^2}\right)} \tag{4.7}$$

where A is the amplitude of the input signal and T_0 is the half width. By definition, the relation between T_0 and half width full maximum (HWFM) T_{HWFM} is given as

$$T_{HWFM} = 2\left(\ln 2\right)^{\frac{1}{2}} T_0 \approx 1.665 T_0 \tag{4.8}$$

The Fourier transform of input signal in frequency domain is

$$\widetilde{S}(0,\omega) = \int_{-\infty}^{+\infty} S(0,T) e^{j\omega T} dT \tag{4.9}$$

Substitute Equation 4.7 into the above equation, we get

$$\widetilde{S}(0,\omega) = \int_{-\infty}^{+\infty} A e^{\left(-\frac{T^2}{2T_0^2}\right)} e^{j\omega T} dT \tag{4.10}$$

Since the inverse group velocity β_1 is set to 0, the transfer function of fibre is given in Equation 4.5 becomes $H(\omega) = e^{\frac{1}{2} j\beta_2 \omega^2 z}$. Thus the output signal in frequency domain is just the multiplication of $\widetilde{S}(0,\omega)$ and $H(\omega)$, which is apprently

$$\widetilde{S}(0,\omega) = A T_0 e^{\left[-\left(\frac{T_0^2}{2} - \frac{j\beta_2 z}{2}\right)\omega^2\right]} \tag{4.11}$$

Perform Fourier transform on Equation 4.11, and the output signal in time domain is

$$\begin{aligned} S(z,T) &= \frac{1}{2\pi} \int_{-\infty}^{+\infty} \widetilde{S}(z,\omega) e^{-j\omega T} d\omega \\ &= \frac{1}{2\pi} \int_{-\infty}^{+\infty} A T_0 e^{\left[-\left(\frac{T_0^2}{2} - \frac{j\beta_2 z}{2}\right)\omega^2\right]} e^{-j\omega T} d\omega \end{aligned}$$

Apparently, the output signal after transmitting through a fibre of length z can be simplified and rewritten as

$$S(z,T) = \frac{AT_0}{\sqrt{T_0^2 - j\beta_2 z}} e^{\left[-\frac{T^2}{2\left(T_0^2 - j\beta_2 z\right)}\right]} \tag{4.12}$$

In Figure 4.4, $\beta_2 = -2100\ ps^2/km$ and $\beta_2 = -4200\ ps^2/km$ are used to calculate $S(z,T)$ by Equation 4.12. The dispersion length L_D=11.44km and 5.72km. The fibre length z is set to be 20km ($> L_D$) in the simulation to guarantee the visibility of broadening. The results shown in Figure 4.4 and 4.3 are identical, and both of them give a rough idea of how the dispersive broadening can distort the signal transmitted through the optical fibre.

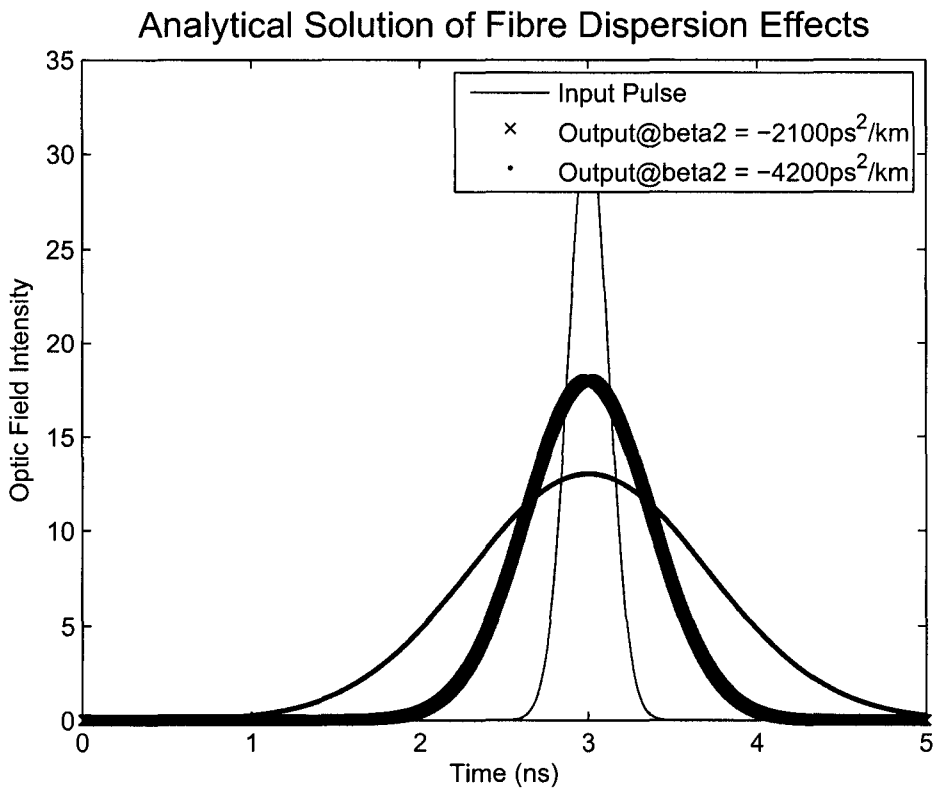

Figure 4.4: Analytical solution of fibre dispersion effects with two sets of dispersion coefficient values: $\beta_2 = -2100\ ps^2/km$ and $\beta_2 = -4200\ ps^2/km$

If the output optic pulse of FP multimode laser diode is fed into the fibre length of 5km, with the parameters given in Table 4.1 the output is slightly distorted as shown in Figure 4.5.

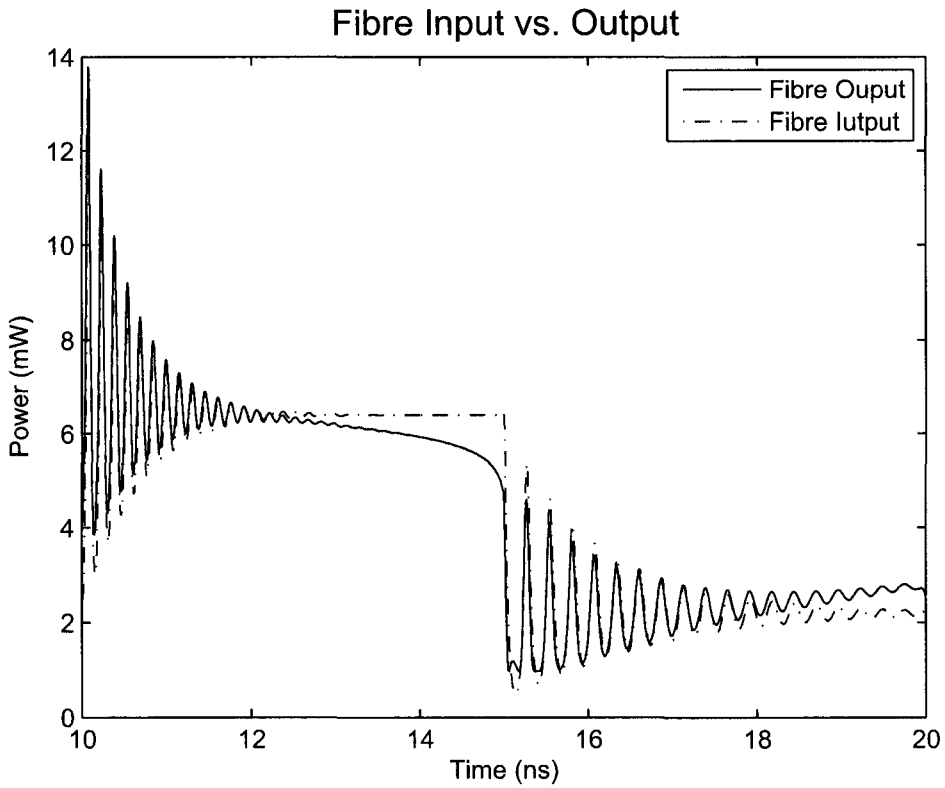

Figure 4.5: Total optical waveform transmitted through a 5km fibre compared with input signal (solid line represents output)

4.2 PIN Photodiode

As indicated by PIN photodiode structure shown in Figure 4.6, a wide intrinsic region is inserted between P and N type semiconductors. The intrinsic region

marked as "Depletion Region" also extends into both P and N junctions, which is denoted as "i" marked in Figure 4.6.

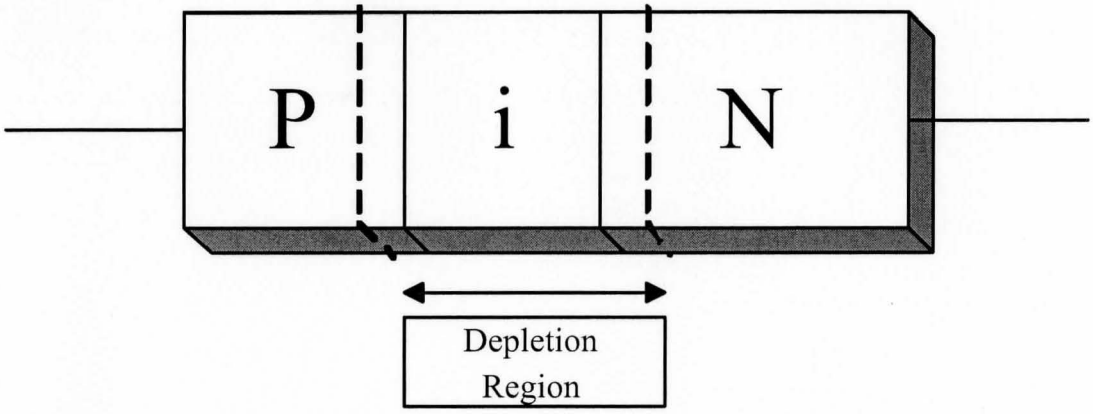

Figure 4.6: PIN photodiode structural layers

According to ECE756 course notes written by Dr. Kumar ([9]), the PIN photodiode can be modeled as a low pass filter (LPF) with a bandwidth ω_{BW}, thus the transfer function can be derived as $H(\Omega) = \frac{1}{1+j\frac{\omega}{\omega_{BW}}}$. The bit rate is limited by its rise time τ_{tr}, which is given by $\tau_{tr} = \frac{w}{v_d}$, where w is depletion region width and v_d is called the drift velocity.

The numerical model of photodiode is relatively straight forward here. Its transfer function is exactly an LPF. The total output optic signal of the laser is approximately an exponential decay with high frequency oscillations. Theoretically, by setting proper bandwidth, the photodiode should filter out these oscillations. The simulation result verifies this speculation as shown in Figure 4.7. The solid line is the output electric signal of the photodiode and the dashed line represents the optic signal respectively. Figure 4.8 shows the detailed output signal of main and side modes. Note that the vertical coordinate on the left hand side is for photodiode output plot. The output intensity is reduced to be almost half of the input

signal of the photodiode.

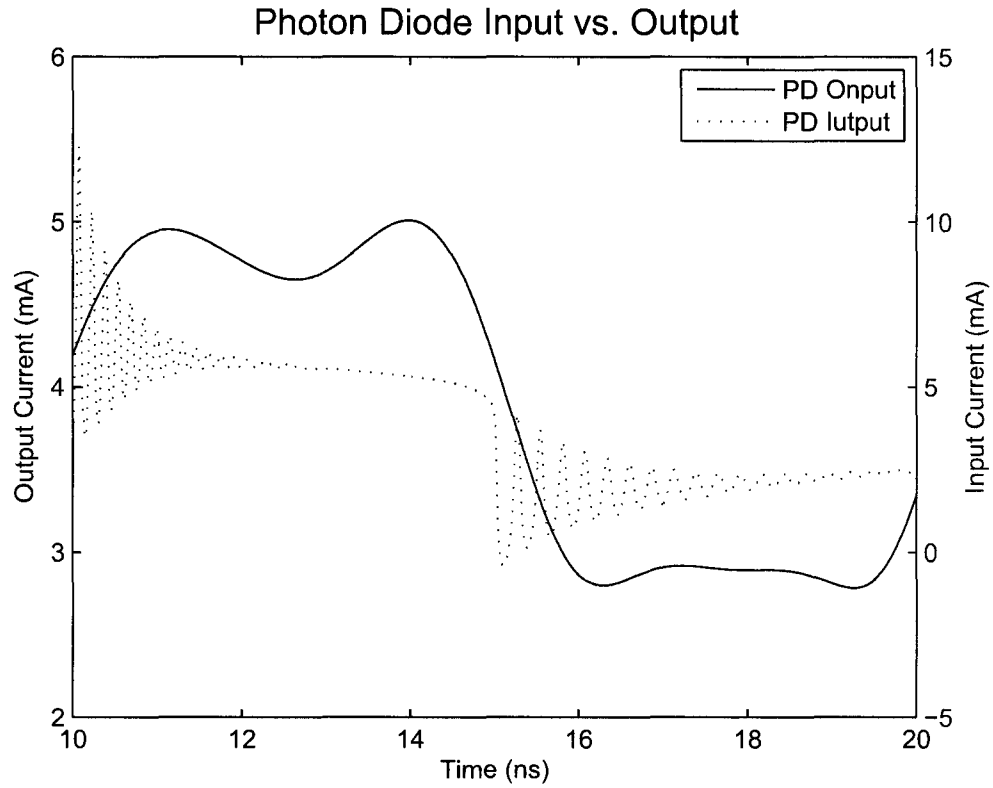

Figure 4.7: Output electric signal of photodiode vs. its input signal (solid line is output waveform of the photodiode)

Since the ultimate objective is to measure and calculate the system performance, the noise on receiver side cannot be neglected. Generally the receiver noise consists of two parts: shot noise and thermal noise. If optic signal power is given as P_0 and responsivity is R, the detected current can be written as

$$I(t) = I_P(t) + i_S(t) + i_T(t)$$

where $I_P(t) = RP_0$ is the optic current, $i_S(t)$ is the noise component due to shot

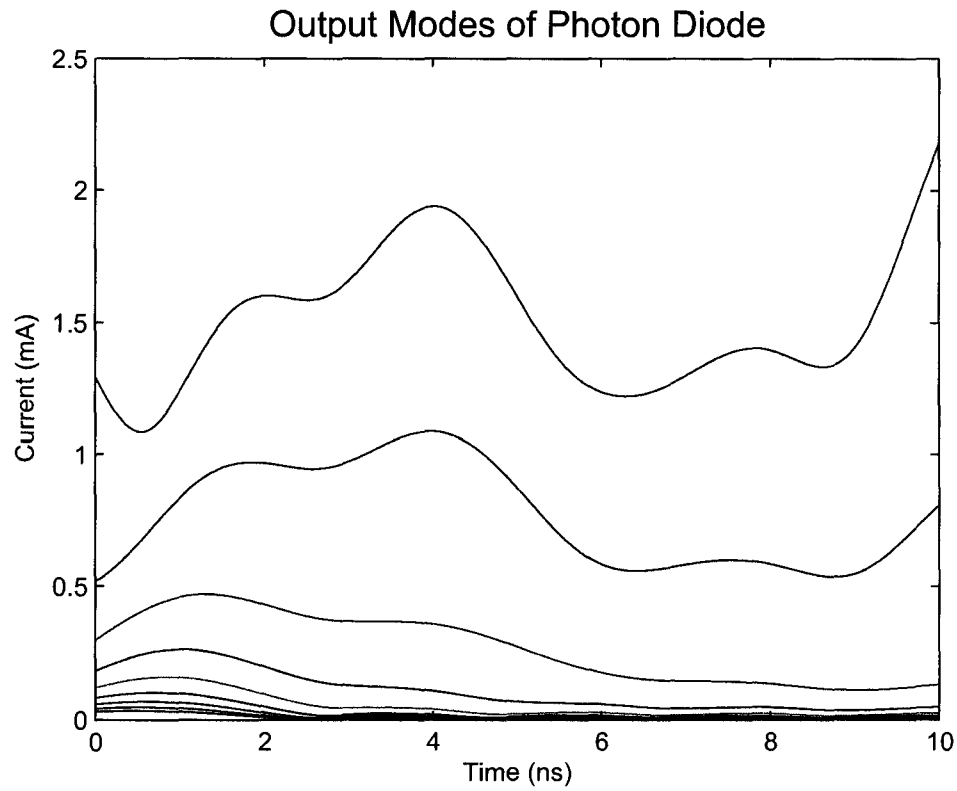

Figure 4.8: Signal received by photodiode, showing details on main and side modes

noise and $i_T(t)$ is the noise component due to thermal noise.

Shot noise is a type of electronic noise that occurs on the receiver side when a finite number of photon fluctuations influence the statistical measurement. If the load resistance is assumed to be R_L, the shot noise average power is given by

$$N_S = E\left\{i_S^2(t)\right\} R_L = \sigma_S^2 R_L \tag{4.13}$$

where σ_S is the standard deviation. The signal power can be easily written as $S = I_P^2 R_L = (RP_0)^2 R_L$. Apparently, the signal to noise ratio associate with shot

noise denoted as SNR_S is given by

$$SNR_S = \frac{S}{N_S} = \frac{(RP_0)^2}{\sigma_S^2} \tag{4.14}$$

The next step is to derive the expression for the standard deviation . The shot noise is a white noise, whose power spectral density (PSD_S) is given by $PSD_S = qL_PR_L$. Since it is assumed previously that photodiode can be treated as a low pass filter with transfer function $H(f)$ and bandwidth Δf. Therefore, the output noise average power N_S can be written in another way

$$\begin{aligned} N_S &= \int_{-\infty}^{+\infty} PSD_S(f)|H(f)|^2 df \\ &= qI_PR_L \int_{-\infty}^{+\infty} |H(f)|^2 df \\ &= 2qI_PR_L\Delta f \end{aligned} \tag{4.15}$$

Now let Equation 4.13 equals 4.15, we get , and Equation 4.14 the signal to noise ratio due to shot noise can eventually be derived as

$$SNR_S = \frac{RP_0}{2q\Delta f} \tag{4.16}$$

The thermal noise is generally caused by random movement of electrons, and it is highly dependent of the temperature. Similar to the shot noise, thermal noise is white noise and its power spectral density (PSD_T) is given by $PSD_T(f) = 2K_BT$, where KB is Boltzman's constant and T is absolute temperature. As a result, the average thermal noise power can be written as

$$\begin{aligned} N_T &= \int_{-\infty}^{+\infty} PSD_T(f)df \\ &= (2K_BT)\,2\Delta f \\ &= 4K_BT\Delta f \end{aligned} \tag{4.17}$$

Similarly, $N_T = E\{i_T^2(t)\} = \sigma_T^2 R_L$, and together with Equation 4.17, the standard deviation for thermal noise is given by $\sigma_T^2 = \frac{4K_BT\Delta f}{R_L}$. Thus, the signal to noise ratio associate with thermal noise (SNR_T) can be written as

$$SNR_T = \frac{S}{N_S} = \frac{(RP_0)^2}{4K_BT\Delta f} \tag{4.18}$$

Consequently, the total signal to noise ratio due to photodiode shot and thermal noise can be expressed as

$$SNR = \frac{(RP_0)^2 R_L}{(2qI_PR_L + 4K_BT)\Delta f} \tag{4.19}$$

In order to more accurately model this fibre-optic system, the shot and thermal noise will be taken into account in the calculation of system power penalty.

4.3 System Performance Analysis

The entire systematic simulation is generated by connecting different components, noise driven FP multimode laser diode, single mode fibre and PIN photodiode together. The BER, Q factor, and power penalty will be measured and eye diagram will be plotted with a window width of 3 bits. Then these simulation results will be

compared with the analytical approximation based on previous discussion, such as power penalty calculation using Equation 3.23.

The plot of photodiode output versus laser output waveform is shown in Figure 4.9 for comparison with Figure 4.7. The eye diagram is simulated for a bit sequence of 10^6 and window width is set to be 3 bits (3000 sampling points).

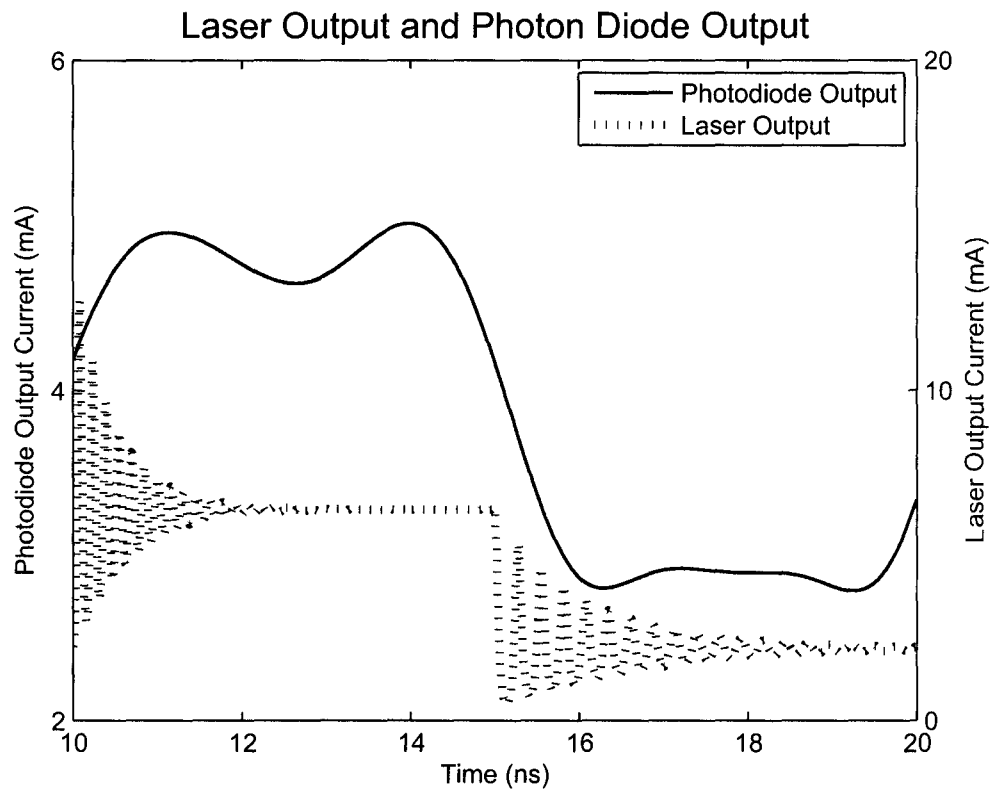

Figure 4.9: Photodiode Output vs. Input

The analytical method of calculating MPN power penalty has been illustrated in Chapter 3, and since the simulation system is constructed with complete components of transmitter, channel and receiver, it is time to demonstrate the idea of numerical solution.

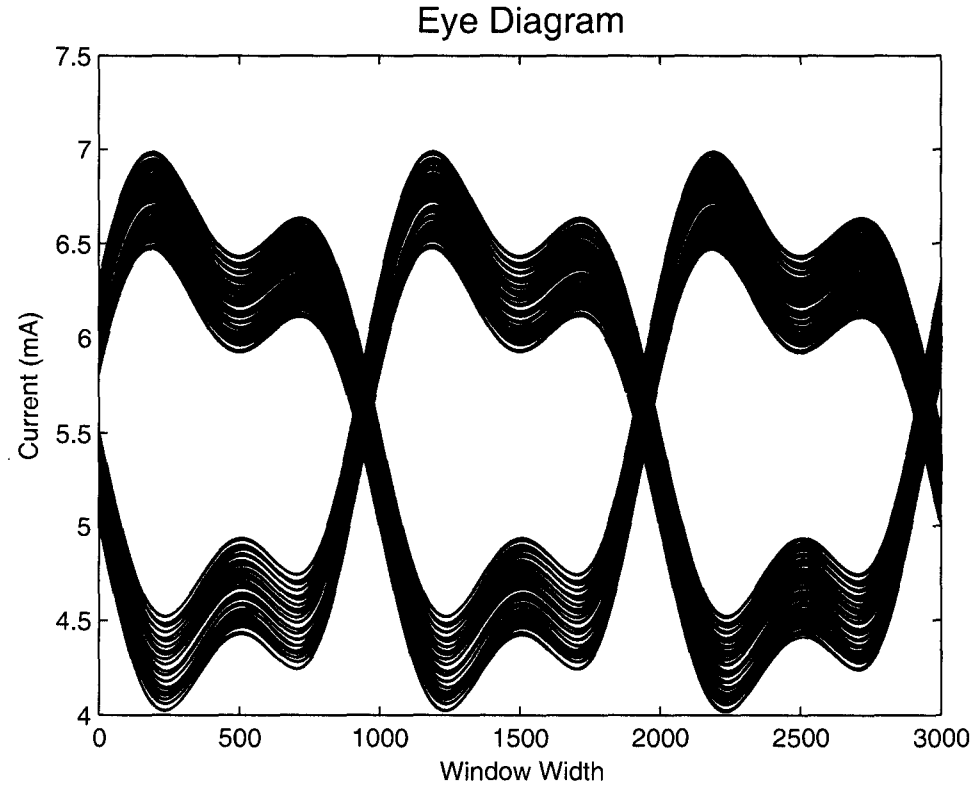

Figure 4.10: Eye Diagram

Recall Equation 3.17, in which $\overline{A_i}$ and $f(\lambda_i, t_0)$ represent the power distribution spectrum and received signal waveform at decision point correspondingly. In the scope of simulation, if t_0 (the decision point) is chosen, $f(\lambda_i, t_0)$ is a sequence of known numbers representing at each decision point the received signal intensity for each mode lasing at certain wavelength λ_i. The value of A_i can be approximated as the power distribution weight of each mode contributing to the total power at the same decision time. Since both $\overline{A_i}$ and $f(\lambda_i, t_0)$ can be either picked up or calculated from the simulation data pool, the MPN power penalty can be easily computed based on Equation 3.17 and 3.19.

The noise driven multimode rate equations are directly modulated. If the MPN coefficient k is taken as $k = 0.5$ or 0.7 ([5]), the received MPN variance σ^2_{MPN} can be solved by 3.17. A sequence train of 10^6 bits is generated to modulate the optic signal, and BER of the received signal is always in the order of 10^{-9}, whose corresponding Q factor is 6.007 from Table 3.2.

MPN power penalty in dB versus fibre length is plotted in Figure 4.11. The dashed line shows numerical results simulated based on the above description and the dotted line is the analytical results stated previously in Chapter 3 respectively.

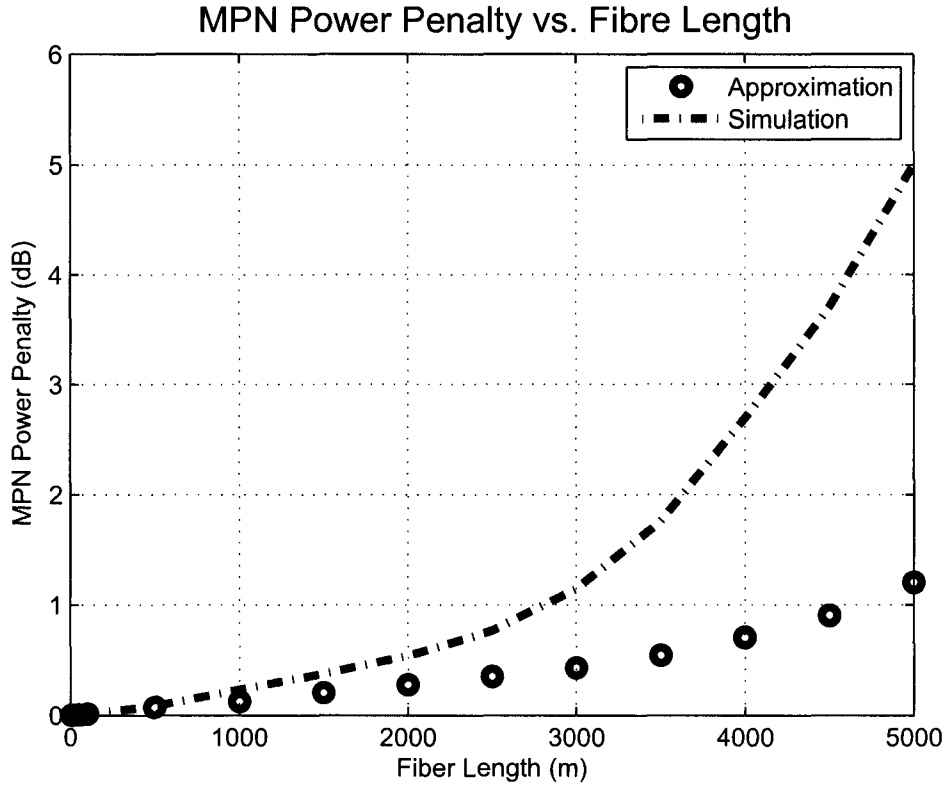

Figure 4.11: Plot of MPN power penalty vs. fibre length: Gaussian-shaped distribution, $k = 0.5$, $M = 17$ modes, and central wavelength lasing at 1310nm

From Figure 4.11 the simulation and approximation show a high level of similarity within a length of 2km. However, the simulation model has a much rapidly increasing power penalty when the fibre length is greater than 2km.

These results illustrate the inadequate approach of analytical modeling of MPN power penalty, which depends on shape of power distribution spectrum, number of modes, length of fibre, and pattern of signal waveform. However, since the simulation results are raw data and the analytical theory is based on optimizing the system by assuming the existence of an equalizer, the realistic performance could be enhanced to approach theoretical standard.

Chapter 5

Conclusion and Future Works

This work establishes a complete numerical model of noise driven FP multimode laser diode rate equations. With connecting to a single mode fibre and PIN photodiode, it forms a basic optical communication system with laser as the transmitter, fibre as the channel and photodiode as the receiver. The focus of problems caused by multi wavelength transmission is to analyze the mode partitioning effects, which can cause intersymbol interference, system power penalty, signal distortion and etc. Additionally, a simple improvement is developed to critically refine the system performance.

There are certainly some works can be done in the future. With absence of a optical amplifier, the signal intensity is greatly reduced after going through the photodiode. To complete the system, an optical amplifier is usually applied in reality. However, it not only enlarges the signal but also the noise. In this case, developing another method of improvement becomes a necessity, such as modification on modulation scheme, application of an equalizer and a mode lock device.

Bibliography

[1] Marcuse, D., & Lee, T. P. (1983). On Approximate Analytical Solutions of Rate Equations for Studying Transient Spectra of Injection Lasers. *IEEE Journal of Quantum Electronics, 19*(9), 1397-1406.

[2] Marcuse, D., & Lee, T. P. (1983). Computer Simulation of Laser Photon Fluctuations: Theory of Single-Cavity Laser. *IEEE Journal of Quantum Electronics, 20*(10), 1139-1148.

[3] Marcuse, D. (1984). Computer Simulation of Laser Photon Fluctuations: Single-Cavity Laser Results.*IEEE Journal of Quantum Electronics, 20*(10), 1148-1155.

[4] Agrawal, G. P., & Dutta, N. K. (1993). *Semiconductor Lasers (2nd ed.)*. New York, NY: Van Nostrand Reinhold.

[5] Agrawal, G. P., Anthony, P. J., & Shen T. M. (1988). Dispersion Penalty for 1.3-um Lightwave Systems with Multimode Semiconductor Lasers. *Journal of Lightwave Technology, 6*(5), 620-625.

[6] Pepeljugoski, P. K., & Kuchta, D. M. (2003). Design of Optical Communications Data Links. *IBM Journal of Res. & Dev., 47*(2/3), 223-237.

[7] Ogawa, K. (1985). Semiconductor Laser Noise: Mode Partition Noise. *Semiconductors and Semimetals, 22*(C), 299-331.

[8] Anderson, T. B., & Clarke, B. R. (1993). Modeling Mode Partition Noise in Nearly Single-Mode Intensity Modulated Lasers. *IEEE Journal of Quantum Electronics, 29*(1), 3-13.

[9] Kumar, S. (2006). ECE756: Design of Lightwave Communication Systems and Networks.

[10] Agrawal, G. P. (2001). *Nonlinear Fiber Optics (3rd ed.)*. San Diego, CA: Academic Press.

[11] Peucheret, C. (2006). Direct Current Modulation of Semiconductor Lasers. *Optical Communication course notes.*

[12] Linke, R. A., Kasper, B. L., Burrus, C. A., Kamnow, I. P., Ko, J. S., & Lee, T. P. (1985). Mode Power Partition Events in Nearly Single-Frequency Lasers. *Journal of Lightwave Technology, 3*(3), 706-712.

[13] Cartledge, J. C. (1988). Performance Implications of Mode Partition Fluctuations in Nearly Single Longitudinal Mode Lasers. *Journal of Lightwave Technology, 6*(5), 626-635.

[14] Nguyen, L. V. T. (2002). Mode-partition Noise in Semiconductor Lasers.

[15] Agrawal, G. P. (2002). *Fiber-Optic Communication Systems*. New York, NY: Wiley-Interscience.

[16] Ogawa, K. (1983). Analysis of Mode Partition Noise in Laser Transmission Systems. *IEEE Journal of Quantum Electronics, QE-18*(5), 849-855.